ANALYTICAL EVALUATION OF THE FLUORESCENCE CHARACTERISTICS OF METABOLITES OF POLYCYCLIC AROMATIC HYDROCARBONS AT ROOM, LIQUID NITROGEN AND LIQUID HELIUM TEMPERATURES

by
KEERTHIKA VATSAVAI
B.S in Pharmacy, Osmania University, India, 2004

A thesis submitted in partial fulfillment of the requirements
for the degree of Masters of Science
in the Department of Chemistry
in the College of Sciences
at the University of Central Florida
Orlando, Florida

Fall Term
2007
Major Professor: Andres D. Campiglia

ABSTRACT

Although environmental monitoring of polycyclic aromatic hydrocarbons (PAH) is an essential step to prevent human exposure to contaminated sites, it provides little information on the actual human uptake and subsequent risks. To this end, urine analysis of short-term biomarkers such as PAH metabolites fill an important niche. The general approach follows the sequence of urine hydrolysis, sample clean-up and pre-concentration, chromatographic separation and determination. Whereas chromatographic methods are based on well established laboratory techniques, the development of easy-to-use, cost-effective and large sample throughput techniques is becoming increasingly relevant to investigate adverse PAH effects on large human populations. This thesis compares the room-temperature, 77K and 4.2K fluorescence properties of 1-naphthol, 2-naphthol, 1-hydroxypyrene, 2-hydroxyfluorene, 3-hydroxybenzo[a]pyrene and 9-hydroxyphenanthrene. These metabolites are used as model biomarkers to investigate the analytical potential of a simple method of analysis based on Solid-Phase Extraction and Room-Temperature Fluorimetry. Metabolites are directly determined in the eluting solvent (methanol) without the need of previous separation via multidimensional formats. Metabolite recoveries varied between 87 ± 1.51% (9-hydroxyphenanthrene) and 99 ± 1.05% (3-hydroxybenzo[*a*]pyrene). For 10mL of urine samples, limits of detection varied between 0.01ng.mL^{-1} (3-hydroxybenzo[*a*]pyrene) and 0.6ng.mL^{-1} (2-hydroxynaphthalene). These figures of merit demonstrate the potential of this approach for screening purposes.

TABLE OF CONTENTS

LIST OF FIGURES

LIST OF TABLES

CHAPTER 1: INTRODUCTION

1.1. General considerations on the analysis of metabolites of polycyclic aromatic hydrocarbons in urine samples

Polycyclic aromatic hydrocarbons (PAH) are important environmental pollutants originating from a wide variety of natural and anthropogenic sources. Generally formed during incomplete combustion of organic matter containing carbon and hydrogen, PAH are omnipresent and abundant pollutants in air, soil, and water. [1] Because many PAH are highly suspect as etiological agents in human cancer, [2] their chemical analysis is of great environmental and toxicological importance. Among the numerous existing PAH, the Environmental Protection Agency (EPA) lists sixteen PAH as "Consent Decree" priority pollutants and recommends their routine monitoring to prevent human exposure to contaminated sites. These include the following: naphthalene, phenanthrene, pyrene, chrysene, 1,12-benzperylene (benzo[*g,h,i*]perylene), dibenz[*a,h*]anthracene (1,2:5,6-dibenzoanthracene), anthracene, acenaphthylene, acenaphthene, fluorene, fluoranthene, 1,12-benzanthracene (benzo[*a*]anthracene), 11,12-benzfluoranthene (benzo[*k*]fluoranthene), 3,4-benzfluoranthene (benzo[*b*]fluoranthene), benzo[*a*]pyrene and indeno[*1,2,3*-cd]-pyrene. Their molecular structures are shown in Table 1.1.

Table 1.1. Structures and Names of Polycyclic Aromatic Hydrocarbons

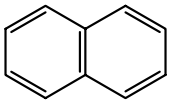

Naphthalene

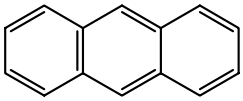

Anthracene

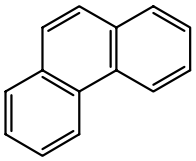

Phenanthrene

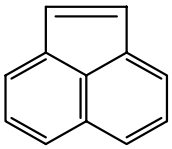

Acenaphthylene

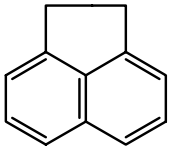

Acenaphthene

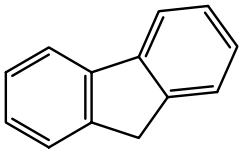

Fluorene

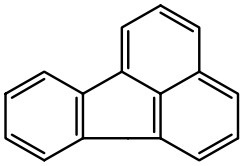

Fluoranthene

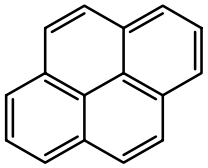

Pyrene

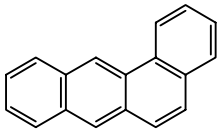

Benzo[a]anthracene

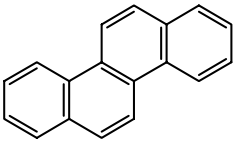

Chrysene

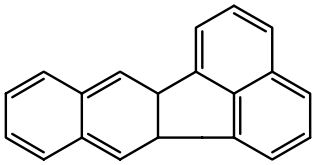

Benzo[k]fluoranthene

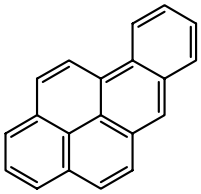

Benzo[a]pyrene

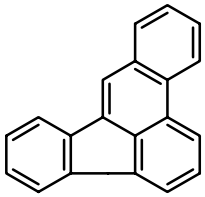

Benzo[b]fluoranthene

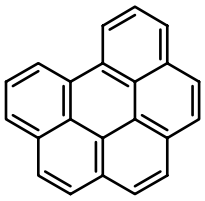

Benzo[g,h,i]perylene

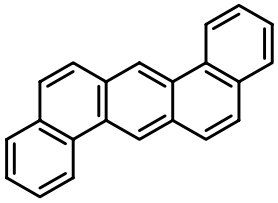

Dibenz[a,h]anthracene

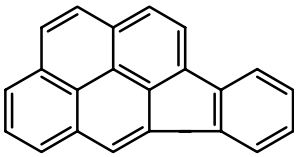

Indeno[1,2,3-cd]pyrene

Although environmental monitoring of PAH is an essential step to prevent human exposure to contaminated sites, it provides little information on the actual human uptake and subsequent risks. To this end, urine analysis of short-term biomarkers such as PAH metabolites fill an important niche. Absorbed into the human body through the skin, lungs and gastrointestinal tract, parents PAH are relatively inert and need metabolic activation to express their carcinogenicity. Because the first step in the metabolic pathway of PAH forms hydroxy-PAH (OH-PAH), urine analysis of OH-PAH is recognized as an accurate assessment of individual's exposure to PAH. [3-7]

Early methods [9-11] focused on the analysis of a few OH-PAH, with particular emphasis on 1-hydroxypyrene. [10] Considering that human exposure often occurs to complex mixtures with numerous PAH, recent methods have expanded their scope to a larger number of metabolites. [6,7] The general approach follows the sequence of urine hydrolysis, sample clean-up and pre-concentration, chromatographic separation and determination. The hydrolysis step – which can be either enzymatic or acidic - is carried out to dissociate OH-PAH from their glucuronide and/or sulfate conjugates. Sample preparation techniques include liquid-liquid extraction, [12] solid-phase extraction (SPE) [3] and solid-phase micro-extraction. [13] Chromatographic separation and determination have been mainly carried out via high-performance liquid chromatography - room-temperature fluorescence spectroscopy (HPLC - RTF) [3, 4] and gas chromatography – mass spectrometry (GC – MS). [6, 7]

Table 1.2 summaries the two analytical figures of merit (AFOM) commonly reported for HPLC and GC analysis of OH- PAH in urine samples. A head-to-head comparison of the analytical recoveries is only possible for those metabolites with

reported values via the two methods, i.e. 2-naphthol, 2-hydroxyfluorene, 9-hydroxyphenanthrene, 3-hydroxyphenanthrene and 1-hydroxypyrene. Apparently, GC-MS provides better recoveries for 2-naphthol, 2-hydroxyfluorene and 3-hydroxyphenanthrene. 9-hydroxyphenanthrene and 1-hydroxypyrene presented approximately the same recovery via HPLC and GC analysis.

Table 1.2. Analytical Figures of Merit commonly reported for HPLC and GC-MS

PAH metabolite	HPLC		GC-MS	
	REC [a] (%)	LOD (pg/mL)	REC [b] (%)	LOD (pg/mL)
1-naphthol	n/a	n/a	78[6], 97[7]	6.2[6] ,15.8[7], 0.33[8]
2-naphthol	82[3]	730[3]	99[7]	2.4[6], 10.5[7], 0.28[8]
9-hydroxyfluorene	n/a	n/a	n/a	2.8[6]
3-hydroxyfluorene	n/a	n/a	n/a	2.0[6], 1.5[7]
2-hydroxyfluorene	62[3]	720[3]	82[6]	3.6[6], 1.5[7]
4-hydroxyphenanthrene	n/a	n/a	n/a	5.7[6], 0.78[7]
9-hydroxyphenanthrene	96[3]	160[3]	93[7]	3.1[6], 0.78[7], 0.45[8]
3-hydroxyphenanthrene	77[4]	10[4]	95[6], 103[7]	3.6[6], 0.78[7], 2.64[8]
1-hydroxyphenanthrene	96[3]	160[3]	n/a	3.5[6], 0.78[7]
2-hydroxyphenanthrene	n/a	n/a	n/a	3.2[6], 0.78[7]
1-hydroxybenzo[*c*]phenanthrene	n/a	n/a	n/a	3.4[6], 1.38[7]
2-hydroxybenzo[*c*]phenanthrene	n/a	n/a	n/a	5.4[6], 1.38[7]
3-hydroxybenzo[*c*]phenanthrene	n/a	n/a	73[6]	5.4[6], 1.38[7]
1-hydroxypyrene	83[3],85[5], 93[4]	40[3],5[5], 4 [4]	80[6], 99[7]	3.3[6], 1.6[7], 1.31[8]
1-hydroxybenz[*a*]anthracene	n/a	n/a	94[6]	3.9[6], 1.32[7]
3-hydroxybenz[*a*]anthracene	77[4]	8[4]	n/a	10.0[6], 1.47[7]
9-hydroxybenz[*a*]anthracene	n/a	n/a	n/a	10.0[6]
4-hydroxychrysene	n/a	n/a	n/a	2.8[6]
6-hydroxychrysene	n/a	n/a	76[6]	2.4[6], 1.68[7]
3-hydroxychrysene	n/a	n/a	70[6]	8.3[6], 1.68[7]
1-hydroxychrysene	n/a	n/a	n/a	5.0[6]
2-hydroxychrysene	n/a	n/a	n/a	5.0[6]
3-hydroxybenzo[*a*]pyrene	45[3],84[4], 48[5]	161[3], 120[4],6[5]	n/a	10.0[6]

[a] REC = Analytical recovery. [b] LOD = Limit of Detection. Reported values are based on 10mL of urine sample.

Unfortunately, the standard deviations of the analytical recoveries were not reported, which make difficult the statistical comparison of the observed differences in their average values. The best limits of detection (LOD) were clearly obtained via GC-MS. Unfortunately GC-MS procedures are more complicated than HPLC methodology. [6, 7] GC-MS requires a chemical derivatization step prior to metabolite separation to avoid peak tailing in the chromatographic column.

Although chromatographic techniques provide reliable results in the analysis of OH-PAH, their experimental procedures are time consuming and expensive. Elution times of 30-60 minutes are typical and standards must be run periodically to verify retention times. If the concentrations of target species are found to lie outside the detector's response range, the sample must be diluted and the process repeated. On the other end of the concentration range, many samples are "zeroes," i.e. the concentrations are below detection limits. Additional problems arise when laboratory procedures are scaled up to handle thousands of samples under mass screening conditions. Unfortunately, there is currently no way to tell beforehand whether the sample merits the full-blown chromatographic procedure.

It is within this context that new analytical approaches based on easy-to-use and cost-effective methodology that provide large sample throughput become extremely relevant. The research presented here points towards the development of screening methodology for the routine analysis of PAH metabolites in numerous samples. It compares the room-temperature fluorescence properties of 1-naphthol, 2-naphthol, 1-hydroxypyrene, 2-hydroxyfluorene, 3-hydroxybenzo[a]pyrene and 9-hydroxyphenanthrene. These metabolites are used as model biomarkers to investigate the

analytical potential of a simple method of analysis based on Solid-Phase Extraction and Room-Temperature Fluorescence spectroscopy (SPE-RTF). Metabolites are directly determined in the eluting solvent (methanol) without the need of previous chromatographic separation. The excellent recoveries and limits of detection presented here demonstrate the potential of SPE-RTF for screening purposes of large number of samples. The fluorescence properties of these metabolites are further investigated at 77K and 4.2K. We demonstrate significant resolution improvements in fluorescence spectra when PAH metabolites are frozen in an alcohol matrix of appropriate molecular length. In addition to improving spectral resolution, lowering the temperature to 4.2K enhances fluorescence intensity and improves limits of detection. These new findings provide a solid foundation to pursue Laser-Excited Time-Resolved Shpol'skii Spectroscopy (LETRSS) for the selective analysis of PAH metabolites in complex physiological samples.

The remaining of this chapter is then devoted to cover the basic principles of the techniques employed in these studies, namely SPE, RTF and LETRSS.

1.2 Solid Phase Extraction

SPE concentrates and purifies analytes from solution by sorption on a solid-surface. The analytes is distributed between the liquid sample and the solid-surface; equilibrium is set up either by simple adsorption to the surface or through penetration of the outer layer of molecules on the surface.

1.2.1 Effectiveness of SPE

An important characteristic for the effectiveness of a solid-phase extraction is the breakthrough volume. The breakthrough volume (V_B) corresponds to the largest sample

volume that can be processed without significant loss of analyte on the sorbent. It can be measured by monitoring the ultraviolet signal of a water sample spiked with traces of a solute, S, which has a initial absorbance, A_0. The spiked sample is passed through a SPE column. If the compound is retained by the sorbent, the effluent will have an absorbance of zero. A breakthrough curve is recorded beginning at a volume, V_B, usually defined a 1% of A_0, up to a volume of V_m, defined as 99% of A_0, where the effluent has the same composition as the spiked water sample. The breakthrough volume is the key for the preconcentration of solute in the SPE.

The V_B for the analyte in the sampling system can be influenced by three parameters: capacity factor, kinetic properties, and retention. The capacity of the sorbent is the number of available sorption sites for the analyte and other retained matrix components. The saturation of these sites leads to the breakthrough, which is related to the mass overload. The capacity of a typical chemically bonded sorbent is 1-10% (w/w), a limit that is unlikely to be exceeded during trace enrichment of samples. Kinetic parameters, such as the sampling bed and the sample-processing rate, influence the V_B through the dependence of the number of theoretical plates on them. The retention factor is given by the partition coefficient.

The breakthrough volume can be defined as

$$V_B = V_R - 2\sigma_{v,} \quad (1)$$

where V_R is the retention volume of the analyte in the sorbent and σ_v is the standard deviation of the axial dispersion along the sorbent bed.

$$V_R = V_0 (1+K') \quad (2)$$

$$\sigma_v = V_0 (1+K')/\sqrt{N}, \quad (3)$$

where V_0 is the hold up volume, K′ is the capacity factor, and N is the number of theoretical plates for the sorbent bed.

$$V_B = [1-3/\sqrt{N}]\ V_0\ (1+K') \quad (4)$$

The dispersion, $\sigma_{v,}$ should be as small as possible, giving the largest V_B. The standard deviation will be minimum if N is increased. Hence, SPE materials within finer sorbent particles would be preferred to achieve larger breakthrough volumes. Numerical evaluation of SPE membranes shows that there is an optimum flow rate range (10-30 mL/min), where the V_B reaches a maximum. For a fixed V_0 and a narrow range of flow rate, the K′ is the dominant parameter that influences different analytes in the sample. An appropriate sorbent gives complete retention of the solute for a good recovery in the extraction.

1.2.2 Solid-Phase Extraction Mechanisms

The three principal mechanisms for concentration and isolation by SPE are normal-phase, ion exchange, and reversed-phase. The normal-phase mechanism involves the sorption of a functional group of the solute by a polar site on the extraction surface. The sorption can occur by hydrogen bond, dipole-dipole, π-π, and induced-dipole interactions. Common sorbents for normal-phase SPE are silica gel, florisil, alumina, amino, cyano, and diol functional groups chemically bonded to silica gel. [14]

The ion-exchange mechanism involves the ion exchange of a charged organic solute from a polar or nonpolar solvent onto the oppositely charged ion-exchange sorbent. The ion exchange resin consists of an ion-exchange group attached to a polymeric matrix or silica-bonded phase. The greater the charge of the analyte being

exchanged, the more tight bound the ion is. Common sorbents for ion-exchange SPE are carboxylic acid, sulfonic acid, and quaternary amines.

The reversed-phase mechanism involves partitioning the organic solute from a polar mobile phase, such as water, into a nonpolar phase. The mechanism of isolation is a nonpolar interaction, Van der Waals forces. Reversed-phase sorbents are commonly used in SPE when aqueous samples are involved.

1.2.3 Reversed-Phase Mechanism

In the reverse-phase process, the analyte will pass into the solid surface, and given time, the equilibrium will be established between the two phases. The equilibrium is described by the partition coefficient for the analyte, which is simply the ratio of concentrations for the analyte in the two phases. The basic concept for the partition mechanism is dictated by the difference in chemical potential of the solute between the stationary (sorbent) and mobile phase (solvent). It reflects the affinity of the solute to the phase and it s solubility. [15]

The chemical equation is given by

$$\mu_i^s = (\mu_0)_i^s + RT\ln C_i, \quad (5)$$

where μ_i^s is the chemical potential of solute, i present in the solvent phase, $(\mu_0)_i^s$ is the standard chemical potential of solute, i present in the solvent phase, and C_i is the concentration of solute.

At the equilibrium, the chemical potential in both phases will be the same.

$$\mu_i^s = \mu_i^b, \quad (6)$$

where μ_i^s is the chemical potential of solute, i, present in the solvent phase and μ_i^b is the chemical potential of solute, i, present in the sorbent phase.

The partition coefficient dictates the distribution of the solute between the solid sorbent and the solvent. The larger the partition coefficient, the better the retention of solute in the solid phase. It can be represented by

$$C_i^b / C_i^s = \exp [-\Delta\mu^0_i/RT] \quad (7)$$

$$K = C_i^b / C_i^s \quad (8)$$

The affinity of the solute for the reversed-phase sorbent can be directly estimated by the partition coefficient. Common sorbents for reversed-phase SLE are alkyl and aryl groups bonded to a silica surface.

1.2.4 Solid-Phase Extraction Protocol

The solid-phase extraction process can be divided in four steps: conditioning, retention, rinsing and drying. [14-17] The silica sorbent must undergo proper conditioning to wet the packing material before the sample passes through the SPE device. In its dry form, the C_{18} bonded-phase material is randomly oriented on the surface. If the sorbent is placed in contact with an aqueous sample, the environment surrounding the bonded organic moiety would be highly polar. Such an environment would be entirely incompatible with a C_{18} bonded-phase. These materials are completely immiscible with each other. The bonded groups try to minimize the exposure to the high polarity medium by forming clusters among them that are close to each other. In such a configuration, the organic surface that is exposed to the solute is very small. This arrangement of the bonded organic groups diminished the SPE process efficiency. In this process, the nonpolar sorbent is activated by treatment with an organic solvent, typically methanol. Under these conditions, the bonded-organic moiety is more open and available

for interaction with the solute. This process can be determined as one of the most important step for a successful SPE.

After the conditioning, the sample and analyte are loaded to the SPE by gravity feed, pumping, or aspirated by vacuum. Depending on the type of sample, micro liters to liters can be applied through the membrane. During this step, the analyte is concentrated on the sorbent by the mechanisms of retention mentioned before. Some of the matrix components may also be retained, and others may pass through, which gives some purification of the analyte.

The rinsing step is used to remove interferences from the SPE material. The rinsing will remove the sample from the interstitial spaces of the sorbent while retaining the analyte. For aqueous samples, a water-organic-solvent mixture may be used.
The final step is the elution of the analyte from the sorbent with an appropriate solvent that is specifically chosen to disrupt the analyte-sorbent interaction. The elution solvent should remove as little as possible of the other substances sorbed on the column. An important consideration is the removal of water from C_{18} sorbent before the analyte elution. Water is retained in the void spaces of the sorbent as well as adsorbed to the silica surface through hydrogen bonding and dipole-dipole interactions. In order for the elution solvent to wet the bed of the sorbent effectively, the sorbent must be dried. Air or vacuum may be used to remove the water from the sorbent.

1.2.5 Solid-Phase Extraction Material

SPE materials are packed in two formats, discs and cartridges. A SPE cartridge consists of a small column (generally an open syringe barrel) containing a sorbent with an average particle size of 40 μm packed between plastic frits. The sorbent bed occupies

about one-third of the syringe barrel volume. The remainder of the volume is used as sample reservoir. SPE discs are particle-loaded membranes in the form of flexible discs of various diameters and 0.5-1.0 mm of thickness. They are packed in a way that the sorbent is enmeshed into a web of some other inert polymer, e.g., Teflon, or is trapped in a glass fiber or paper filter. SPE discs are preferred over cartridges because their larger cross-sectional area and shorter bed depth allow higher flow rates and shorter analysis time.

The SPE bonded-phase can be prepared by reacting silica gel with an appropriate organic mono-, di-, or trichlorosilane, producing a surface coating of organic material that replaces the hydroxyl groups as the interacting moieties of the stationary phase. The interacting organic groups are hydrocarbon chains. Octadecyl (C_{18}) groups bonded to the silica surface are the sorbents used for most non-polar applications, such as the extraction of metabolites of polycyclic aromatic hydrocarbons. [17]

1.3. Photoluminescence Spectroscopy

1.3.1 Basic Principles Involving Fluorescence and Phosphorescence

Photoluminescence spectroscopy is based on the detection of radiation of 200-700 nm emitted during the deactivation of electronically excited molecules. [18-20] Under normal conditions, the orbital of lowest energy of an organic molecule are occupied by pairs of electrons with spin in opposite directions. [21] Since most of the organic molecules have an even number of valence electrons, the resulting electron spin is zero. Such a state, with no net spin, is called a singlet state. The singlet state of lowest energy is known as the ground state, and it is represented in the Jablonski diagram of Figure 1.1 by S_0.

Through the absorption of electromagnetic radiation (A), a molecule can pass from the ground state to an excited state of higher energy. This transition occurs in approximately 10^{-15} s and entails the promotion of an electron from the highest occupied orbital to a previously unoccupied one. If the transition occurs with no change in the spin of the promoted electron, the excited state will have two unpaired electrons with anti parallel spins and, therefore, net spin equal to zero. An electronic state with these characteristics is known as a singlet excited state. In Figure 1.1, the first and second singlet-excited states are represented by S_1 and S_2, respectively. If the transition involves a change in the electronic spin, the excited state will be characterized by two unpaired electrons with parallel spins. In this case, the resultant spin is one, and the excited state receives the name of triplet state. In Figure 1.1, the triplet state of the lowest energy is symbolized by T_1 while any other triplet state of higher energy is represented by T_n.

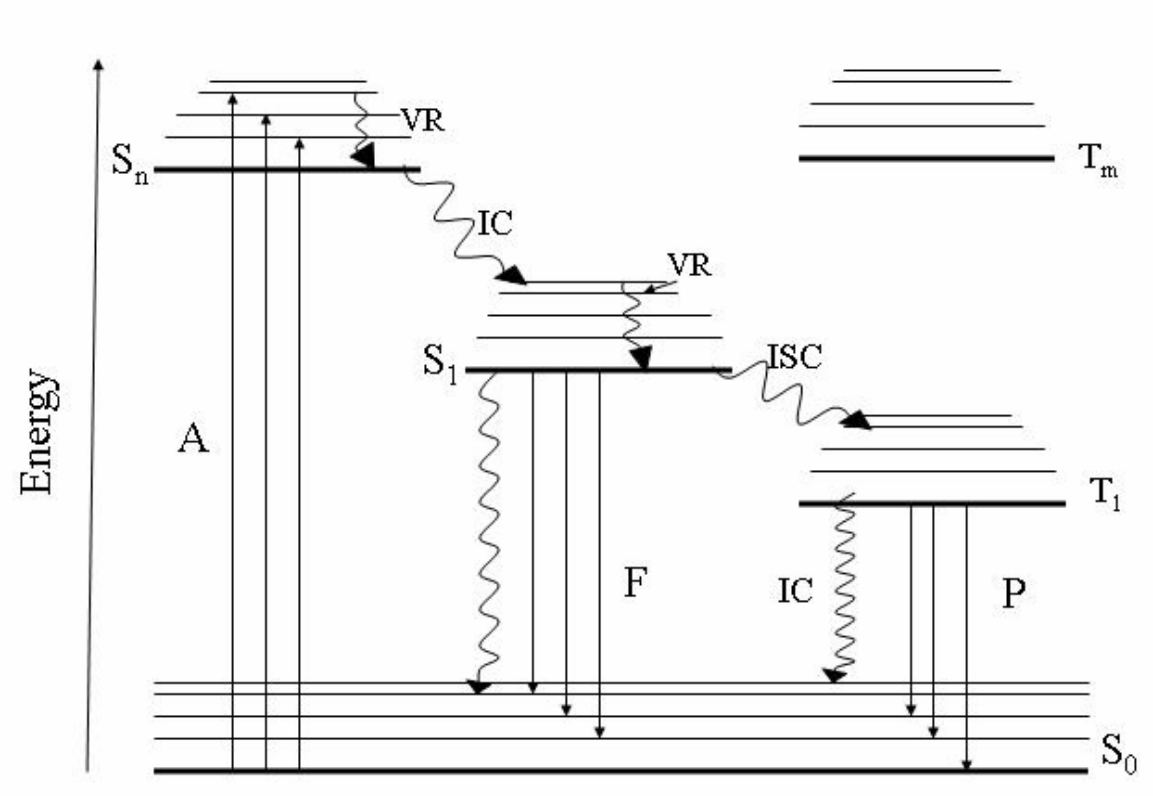

Figure 1.1. Jablonski diagram. A is the absorption, F is the fluorescence, P is the phosphorescence, VR is the vibrational relaxation, IC is internal conversion, and ISC is the intersystem crossing.

When the energy of an absorbed photon is enough to excite a molecule to a state such as S_2, it usually releases the extra vibrational energy to reach the lowest vibrational level of the state. This radiationless deactivation mechanism is known as vibrational relaxation (VR), and it is the consequence of the energy transfer from the excited molecule to the surrounding medium in the form of thermal energy.

Through another radiationless process called internal conversion (IC), the molecule passes from the lowest vibrational level of S_2, a vibrational level of S_1. This process results in the transformation of excitation energy into vibrational-rotational energy [22]

and occurs between electronic states of the same multiplicity. [23] The lowest vibrational level of S_1 is then reached through VR. If the molecule was initially excited to a higher excited state than S_2, the lowest vibrational level of S_1 would be reached by a succession of IC and VR processes. From the lowest vibrational level of S_1, the molecule has two ways of directly returning to the ground state: through IC, without the emission of radiation, or by the mission of a photon with no change in the electronic spin. The latter process is responsible for the emission of fluorescence and occurs in a time period of 10^{-10} to 10^{-7} s. The energy of the emitted photon corresponds to the energy gap between the lowest vibrational level of S_1 and the ground state. When the lowest vibrational level of the S_1 state overlaps with S_0, the excited state is deactivated by nonradiative relaxation, and the emission of fluorescence does not occur.

When the emitted photon has the same energy as the one initially absorbed, the process is termed resonance fluorescence. Most times, however, the energy loss in VR and IC results in the emission of fluorescence at longer wavelengths than the excitation wavelength, and resonance fluorescence is not observed.

The remaining possibility to return to S_0 from S_1 begins with a process called intersystem crossing (ISC). ISC is radiationless mechanism involving systems of different multiplicity which requires a change in the electronic spin. [21] Although this kind of transition has a much lower probability to occur than spin-allowed transition, [20,21] the time scale of ISC is similar to the one for fluorescence (10^{-10} – 10^{-7} s); therefore, it competes with fluorescence for the deactivation of S^1. From S^1, the molecule can then pass to the excited triplet state manifold (T_n) and reach, by a succession of VR an IC processes, the lowest vibrational level of T_1. From T_1, and through ISC, the

molecule can revert back to the excited singlet state manifold. Since the triplet states have lower energy than the corresponding singlet states, the transition from T_1 to S_1 requires some additional activation energy. This activation energy can be obtained either by a thermal process or by the interaction of two molecules in the triplet state to produce one molecule in the excited singlet state. [21, 22] The emission of radiation from the excited S_1 to S_0 receives the name of delayed fluorescence.

If reverse ISC does not occur, the molecule has two additional possibilities to return from T_1 to S_0: through ISC followed by VR or through the emission of radiation in a process called phosphorescence (P). The emission of phosphorescence involves states of different multiplicity and, as a consequence, has a longer lifetime than fluorescence (between 10^{-3} and 10 s). Since the energy gap between T_1 and S_0 is usually smaller than the one between S_1 and S_0, phosphorescence occurs in a region of larger wavelength than fluorescence.

The radiative deactivation processes (fluorescence and phosphorescence) are always in competition with the various non-radiative deactivation processes. The intensity of fluorescence and phosphorescence will then depend upon the relative efficiencies of all competing processes. The efficiencies of fluorescence and phosphorescence are often expressed in terms of quantum yield, ϕ. The quantum yield for fluorescence, ϕ_F, is the ratio of the rate of fluorescence with the rate of absorption, $\mathbf{\Phi}_F$/ $\mathbf{\Phi}_A$, where $\mathbf{\Phi}_F = k_F n_{S1} V$ and $\mathbf{\Phi}_A = k_A n_{S0} V$. V is the volume of sample illuminated; n_{sx} is the number of molecules occupying the given electronic state x; and kF and k_A are the rate of fluorescence and absorption, respectively. Under steady state conditions, we can assume that $n_{s1} = n_{s0} k_A / (k_F + k_{nr})$, where k_{nr} is the sum of rates for the non-radiative

processes (external conversion, k_{ec}; internal conversion, k_{ic}; and inter-system crossing, kisc). Using these relationships, the fluorescence quantum yield in terms of the rates of the various activation and deactivation processes is given by equation (9):

$$\phi_F = \frac{k_F}{k_F + k_{nr}} \tag{9}$$

which shows that, in order to improve the fluorescence quantum yield, and hence the fluorescence intensity, one needs to minimize the rate contributions from non-radiative processes. A similar situation arises for phosphorescence. The phosphorescence quantum yield, ϕ_P, can be expressed as

$$\phi_P = \frac{k_{isc}}{k_{isc} + k_F + k_{nr}} \times \frac{k_p}{k_P + k_{nr}} \tag{10}$$

Note that the first term in equation (10) takes into account the efficiency of inter-system crossing. Therefore, to maximize the phosphorescence efficiency, hence the phosphorescence intensity, minimization of both non-radiative processes and fluorescence relative to inter-system crossing becomes evident.

Because the excited states (S_1 and T_1) are often deactivated by first-order processes, the decay of either fluorescence or phosphorescence can be described by equation (11):

$$I_{(t)} = I^0 e^{-t/\tau_L} \tag{11}$$

where I^0 is the luminescence intensity at time zero and τ_L is the luminescence lifetime. The lifetime is defined as the time it takes for the luminescence to decay to 1/e of its initial value. The lifetimes for fluorescence and phosphorescence are related to the rate constants for deactivation by equations (12) and (13).

$$\tau_F = (k_F + k_{nr})^{-1} \quad (12)$$

$$\tau_P = (k_P + k_{nr})^{-1} \quad (13)$$

Equations (9), (10), (12), and (13) indicate that non radiative decay processes decrease the fluorescence and phosphorescence intensities and lifetimes by the same factor. In other words, the lifetime and the quantum efficiency are proportional to $(k_L + k_{nr})^{-1}$.

1.3.2. Room-Temperature Fluorescence Spectroscopy

The detection of luminescence (fluorescence and/or phosphorescence) is the basis of several photoluminescence techniques. Fluorescent and/or phosphorescent compounds usually consist of molecules with extensive π electron systems. These include a large variety of aromatic molecules either with or without hetero-atoms in the conjugated system. [18-21]. The free movement of π electrons throughout the delocalized molecular orbitals facilitates the electronic transitions responsible for fluorescence and phosphorescence. For molecules with no hetero-atoms in the aromatic system, transitions frequently involve the promotion of an electron from a bonding π orbital to an anti-bonding π∗ orbital (π – π∗ transition). Aliphatic molecules, on the other end, rarely exhibit luminescence since the high energy required for σ – σ∗ transitions usually causes decomposition prior to excitation. [18-21] Among the numerous photoluminescence techniques known in the analytical field, Room-Temperature Fluorescence (RTF) spectroscopy is the most popular. RTF offer the advantages of relatively inexpensive instrumentation, calibration curves with excellent linear dynamic ranges and appropriate

limits of detection. In most cases, de-oxygenation of the sample is not critical and fluorescence measurements are rapidly performed by placing a quartz cell in the sample compartment of a spectrofluorimeter.

Conventional fluorimetric methods - in which either the excitation or the emission wavelength is set at its maximum position while the other is scanned – present limited selectivity. The similarity and/or overlapping of broad fluorescence bands at room-temperature usually interfere in the characterization of targeted compounds without previous separation. Several strategies exist to improve the selectivity of room-temperature fluorescence measurements. These include temporal (lifetime) resolution, [24-26] excitation-emission matrices (EEM) [27,28] and synchronous excitation. [29-31] EEM fluorescence spectroscopy takes full advantage of fluorescence spectra. A fluorescence EEM is obtained by measuring fluorescence intensities for all kinds of combinations of fluorescence emission and excitation wavelengths in a certain wavelength interval. The two (or rather three, since obviously the intensity is the third variable) dimensional information is usually represented in isointensity plots, in which points of equal intensity are connected in a graph with the excitation and emission wavelength (or frequency) as axes. Pseudo-3D plots are also common, in which spectra are viewed as “mountain landscapes” from viewing angles carefully chosen to reveal pertinent spectral details. Although EEM have been applied to environmental analysis of parent PAH, our literature search revealed no applications to the analysis of PAH metabolites in urine samples.

1.4. Shpol'skii Spectroscopy of Metabolites of Polycyclic Aromatic Hydrocarbons

Shpol'skii Spectroscopy has long been recognized for its unique capability of providing efficient and adequate resolution of parent PAH at the concentration ratios found in environmental samples without previous chromatographic separation. Its unique capability results from the unmatched spectral resolution observed in Shpol'skii matrixes. The term Shpol'skii matrix refers to a dilute solution of a guest molecule (PAH) in a solvent host (usually an n-alkane) where the solvent freezes to 77K or below into an ordered polycrystalline matrix. If the dimensions of the analyte and solvent match up well enough, PAH occupy a small number of crystallographic sites (ideally just one) in the host matrix. Matrix isolation of guest molecules reduces inhomogeneous band broadening, which results in vibrationally resolved excitation and emission (fluorescence and/or phosphorescence) spectra with sharp line widths.

Publications describing the use of Shpol'skii Spectroscopy for PAH metabolites are relatively rare. Garrigues and Ewald reported quasi-linear spectra for 9-hydroxybenzo[a]pyrene. [32] Among the OH-PAH included in Karcher's spectral atlas, a Shpol'skii spectrum was included only for 3-hydroxybenzo[a]pyrene. [33] The sensitivity of the Shpol'skii method for phenolic metabolites of benzo[a]pyrene is more than an order of magnitude poorer than the one for benzo[a]pyrene [34], although their room temperature fluorescence quantum yields are similar. In the case of 1-hydroxypyrene, the difference in sensitivity is even larger. [35] Experimental evidence suggests that this phenomenon is caused by the limited host-guest compatibility due to the polar hydroxyl group, the latter having a stronger influence in the case of the four ring pyrene derivative than in the case of the five-ring benzo[a]pyrene derivative.

In principle, two effects can occur, resulting from either the poorer solubility in n-alkanes or the poorer compatibility with the n-alkane crystal lattice. The first is the formation of aggregates during the cooling procedure, leading to precipitation and reduced quantum yields. The second concerns freezing out of the metabolite molecules, at the point of matrix solidification, from the crystalline phase being formed into amorphous, intergrain phase [36], resulting in broadband emission at the expense of the intensity of the Shpol'skii lines. Both phenomena will also cause the intensity and appearance of the Shpol'skii spectrum to depend critically on cooling rate, sample holder design and traces of other solvents. These nuisances significantly hamper analytical reproducibility and inter-laboratory compatibility.

In order to improve the compatibility of PAH metabolites with typical n-alkane Shpol'skii matrixes, Weeks and co-workers [37] first described a procedure to transform monohydroxybenz[a]anthracenes into less polar methoxy derivatives, which could subsequently be analyzed by means of Shpol'skii spectroscopy. Later, the methylation and Shpol'skii spectroscopy analysis of several types of benzo[a]pyrene metabolites was reported, which included monohydroxy-benzo[a]pyrene derivatives, benzo[a]pyrene-dihydrodiols, benzo[a]pyrene-dihydrodiolepoxide and benzo[a]pyrene-tetrahydro-tetrol [34, 38].

Sample extraction and derivatization is carried out as follows: Samples are enzymatically treated to hydrolyze phase II conjugates, and are subsequently extracted with a nonpolar, volatile solvent such as n-hexane. A few mg of sodium hydride is washed with n-pentane in flask under nitrogen atmosphere; dimethyl sulfoxide (DMSO) is added; and the mixture is stirred at 70°C for several minutes until the formation of H_2

bubbles has ceased. After cooling to room temperature, methyl iodide and the sample extract are added; after several minutes of stirring the reaction is quenched with water. The methylated products are quantitatively extracted with n-hexane and concentrated, and the solvent is gradually replaced with n-octane in a gentle stream of nitrogen.

In addition to increasing analysis time, the numerous manual steps of the derivatization procedure increase the probability of metabolite loss and sample contamination. Moreover, the derivatization of polyhydroxylated metabolites provides a mixture of products with relative concentration ratios critically depending on the derivatization conditions. [34,38] For instance, benzo[*a*]pyrene 9,10-dihydrodiol yielded 9-methoxybenzo[*a*]pyrene, 10-metoxybenzo[*a*]pyrene, as well as the expected dimethylated product 9,10-dihydrodimethoxybenzo[*a*]pyrene. The research presented here provides a feasible solution to the problem as it avoids metabolite derivatization prior to Shpol'skii spectroscopy analysis.

CHAPTER 2. EXPERIMENTAL

2.1. Instrumentation

2.1.1. Room-Temperature Fluorescence Spectroscopy.

Steady-state excitation and fluorescence spectra and signal intensities were recorded from un-degassed solutions using a commercial spectrofluorimeter (Photon Technology International). The excitation source was a continuous-wave 75 W pulsed Xenon lamp with broadband illumination from 200 to 2000 nm. The excitation and the emission monochromators had the same reciprocal linear dispersion (4 $nm.mm^{-1}$) and accuracy (±1 nm with 0.25 nm resolution). The gratings (1200 $grooves.mm^{-1}$) were blazed at 300 and 400 nm, respectively. Detection was made with a photomultiplier tube (PMT, model 1527) with spectral response from 185 to 650 nm. The instrument was computer-controlled using commercial software (Felix32) specifically designed for the system.

2.1.2. Laser Excited Time Resolved Shpol'skii Spectroscopy (LETRSS).

The instrumentation for LETRSS was developed in house. Full reports comparing its performance to conventional approaches are available in the literature. Sample excitation was carried out by directing the output of a Northern Lights tunable dye laser (Dakota Technologies, Inc.) through a potassium dihydrogen phosphate (KDP) frequency-doubling crystal. The dye laser was operated on Rhodamine 610 (285-295nm), Rhodamine 640 (300 – 310nm), LDS 6908 (340 – 350nm) and DCM (305 – 330nm). The dye laser was pumped with the second harmonic of a 10 Hz Nd:YAG Q-switched solid-state laser (Big Sky Laser Technologies). Time-resolved fluorescence detection was made with a front-illuminated intensified charge fiber-coupled device (ICCD, Andor

Technology). The minimum gate time full width at half-maximum of the intensifier was 2 ns, and the CCD active area was 690 pixels x 256 pixels (26 nm^2 pixel size photocathode). The ICCD was mounted at the exit focal plane of a spectrograph (SPEX 270M) equipped with a grating (1200 grooves.mm^{-1}) blazed at 500 nm. The system was used in the external trigger mode. The gate delay, width, and step were controlled with a digital delay generator (DG 535, Stanford Research System, Inc.) via a GPIB interface (National Instruments). Custom Labview software (National Instruments) was developed in house for complete instrumental control and data collection.

The cryogenic probe consisted of a fiber optic assembly with one excitation and six collection fibers fed into a 1.25-m-long section of copper tubing that provided mechanical support to lower the probe into the liquid helium. All the fibers were 3 m long and 500 μm core diameter silica-clad silica with polyimide buffer coating (Polymicro Technologies, Inc.). At the analysis end, the excitation and emission fibers were arranged in a conventional six-around-one configuration, bundled with vacuum epoxy (Torr-Seal, Varian) and fed into a metal sleeve for mechanical support. The copper tubing was flared stopping a swage nut tapped to allow for the threading of a 0.75 mL polypropylene sample vial. At the instrument end, the excitation fiber was positioned in an ST connection and aligned with the beam of the tunable dye laser while the emission fibers were bundled with vacuum epoxy in a slit configuration, fed into a metal sleeve, and aligned with the entrance slit of the spectrometer.

2.2 Chemicals and Materials

All chemicals were analytical-reagent grade and were used without further purification. Nanopure water was employed for all the experiments. All the PAH

metabolites were purchased from Sigma-Aldrich at their highest purity except for 3-hydroxybenzo[*a*]pyrene which was purchased from Midwest Research Institute (MRI, Missouri, 64110). Methanol (HPLC grade), hydrochloric acid, potassium biphthalate sodium hydroxide buffer were purchased from Fisher Chemical. Synthetic urine was purchased from Fisher Chemical. The Sep-pak c18 cartridges were purchased from Waters, Milford, MA. Rhodamine 610, Rhodamine 640, LDS 698 and DCM dyes were purchased from Exciton, Dayton, Ohio.

2.3 Procedures and Measurements

2.3.1. Preparation of Stock Solutions of PAH Metabolites.

50μg/mL stock solutions of PAH metabolites were prepared by dissolving 0.5mg of the standard in 10mL of 5% methanol/water (volume/volume, v/v) solution. Stock solutions of intermediate concentration (500ng/mL) were prepared by diluting 100μL of the primary stock solution (50μg/mL) with 10mL of water to obtain a standard solution in 0.05% methanol/water v/v. Stock solutions were kept in the dark at approximately 2.7°C. Intermediate solutions were used to prepare fresh working solutions of PAH metabolites. Prior to use, the fluorescence intensities and spectral characteristics of intermediate stock solutions were monitored for possible photo-degradation of PAH metabolite.

2.3.2. Hydrolysis of Urine Samples.

8mL of synthetic urine sample were spiked with 1mL of metabolite stock solution of appropriate concentration and equilibrated for 30min to allow for the conjugation of OH-PAH with urine components such as urea and various salts. 500μL of 0.1M HCl were added to the sample and the mixture was then buffered with 500μL of 0.05M

potassium biphthalate sodium hydroxide buffer (pH 5.0). The buffered sample was shaken for 30 min at 1400 rpm to allow for urine hydrolysis.

2.3.3. Solid Phase Extraction.

Optimization of experimental parameters concerning the retention and elution of PAH metabolites from the solid-phase cartridge lead to the following procedure: Aqueous metabolite solutions or synthetic urine samples were processed through a sep-pak c18 cartridge previously conditioned with 5mL methanol and 5mLwater. All solutions were processed through the cartridge with the aid of a 10mL syringe attached to the cartridge. The cartridge was sequentially rinsed with 10mL water and 10mL of 20% methanol/water. OH-PAH metabolites were eluted with 3mL of 100% methanol.

2.3.4. Fluorescence Measurements.

Room temperature fluorescence measurements were carried out with commercial instrumentation by pouring un-degassed liquid solutions into standard (1 cm x 1 cm) quartz cuvettes. 77 K fluorescence measurements followed the classic procedure of immersing the undegassed sample solution in a quartz tube into a nitrogen-filled Dewar flask. Measurements at liquid Helium temperature (4.2 K) were performed with the aid of the cryogenic probe and the laser system. Sample freezing was accomplished by lowering the copper tubing into the liquid cryogen. The liquid Helium was held in a Dewar with 60 L storage capacity. Such a volume of liquid Helium would typically last for three weeks of daily use, averaging 15-20 samples/day. Complete sample freezing took less than 90 s. Measurements were made with the tip of the fiber optic probe ~ 0.5 cm above the surface of the frozen sample. The position of the probe was held constant with the screw cap of the sample cell.

2.3.5. Lifetime Analysis at Liquid Helium Temperature.

Fluorescence lifetimes were collected via the WTM procedure, which consisted of the following three steps: (1) collection of full sample and background WTM; (2) subtraction of the background decay curve from the fluorescence decay curve at the wavelength of maximum fluorescence for each PAH; (3) fitting of the background-corrected data to single exponentials. Origin software (version 7, Micro cal Software, Inc.) was used for curve fitting of fluorescence lifetimes. Fitted decay curves ($y = y_0 + A_1 \exp^{-(x-x_0)t_1}$) were obtained by fixing y_0 and x_0 at a value of zero. Otherwise noted, the agreement between the calculated and the observed points over the first two lifetimes of the decays agreed to within about 1% and the residuals showed no systematic trends.

CHAPTER 3. RESULTS AND DISCUSSION

Our literature search revealed numerous SPE procedures for the urine analysis of OH-PAH. Two common features were noted, which refer to the chemical natures of both the solid sorbent and the eluting solvent. OH-PAH are typically extracted from urine samples using commercial cartridges containing silica particles derivatized with C-18 alkyl chains. Independent of the instrumental method, i.e. HPLC or GC-MS, metabolite elution is predominantly carried out with methanol. Only one article uses methylene chloride as eluting solvent, which shows no improvement over methanol elution. [6] Preliminary studies in our lab attempted the SPE of OH-PAH on C-18 extraction membranes. The main goal of these studies was to interface SPE with solid-surface RTF. This approach, which was developed in our lab for water analysis of parent PAH, uses commercial extraction membranes with the dual purpose of analyte extraction and fluorescence measurements. Obtaining fluorescence information directly from the surface of the disk avoids analyte elution and provides a straightforward procedure for rapid determination at low concentration levels. [39-42] OH-PAH studies were then initiated with 1-naphthol and 2-naphthol. Fluorescence intensities of standard aqueous solutions were measured before and after extraction. Because these two metabolites presented rather low retention (~ 30%) on disks, OH-PAH extraction was then pursued with commercial cartridge sorbents using methanol as the eluting solvent.

The six metabolites chosen for these studies were also selected from our literature review (see Table 1.2), as a tentative means of comparing our analytical figures of merit (AFOM) with previously reported data. The efficiency of SPE was investigated in two steps, which monitored the retention and the eluting efficiency of the solid sorbent and

methanol, respectively. The percent of retention (% retention) was calculated according to the formula:

$$\% \text{ retention} = [I_{bef} - I_{aft} / I_{bef}] \times 100 \quad (1)$$

where I_{bef} and I_{aft} refer to the fluorescence intensity of the solution before and after retention, respectively. Keeping in mind that the adsorption of OH-PAH onto the solid sorbent occurs from an aqueous based matrix (urine) and the possibility of matrix interference on the retention of OH-PAH, we first tested their retention from standard solutions in water (methanol/water 0.05% v/v) and then compared their values to the extraction of spiked urine samples. Each OH-PAH concentration used in these studies was within the corresponding linear dynamic range of the calibration curve.

The eluting efficiency (% elution) of methanol was obtained from the following equation:

$$\% \text{ elution} = [\text{Mass eluted} / \text{Mass retained}] \times 100 \quad (2)$$

The mass of eluted OH-PAH was calculated from the product: Mass eluted = V_{eluted} x C_{eluted}, where V_{eluted} is the volume of eluted methanol and C_{eluted} is the concentration of metabolite in the eluted solution. The experimental value of C_{eluted} was obtained from the calibration curve of each OH-PAH in methanol. The mass of retained metabolite was calculated from the product: V_{std} x C_{std} x (% retention), where V_{std} is the volume of standard solution processed through the cartridge, C_{std} is the concentration of standard solution and % retention is the retention efficiency as calculated in equation 1. Because these calculations required the previous knowledge of the spectral characteristics and the AFOM of OH-PAH in water and methanol, fluorescence studies in these directions were then undertaken in both types of solvents.

3.1. Room-Temperature Fluorescence Characteristics of OH-PAH in Water and Methanol

The initial survey of room-temperature excitation and fluorescence spectra was carried out in methanol-water (0.05% v/v) and methanol using a commercial spectrofluorimeter. All spectra were collected using the same excitation and emission bandpass (2nm). No attempts were made to adjust slit-widths to optimize spectral resolution, nor were the spectra corrected for instrumental response. The 2nm bandpass provided signal-to-background ratios higher than 3 ($S/B \geq 3$) for all the studied metabolites at the $ng.mL^{-1}$ concentration level. Figures 3.1 to 3.6 show the blank subtracted spectra of the six OH-PAH in methanol-water (0.05% v/v) (A) and methanol (B) solutions. All standard concentrations are within the linear dynamic ranges (LDR) of the calibration curves. Clearly, the spectral features of the studied metabolites do not change much with solvent composition. This could be attributed to the salvation effect of methanol in the aqueous solution, which might provide a similar micro-environment for each metabolite in both types of solvents. A summary of excitation and fluorescence peaks for each metabolite in methanol-water (0.05% v/v) and methanol is provided in Table 3.1 and 3.2, respectively.

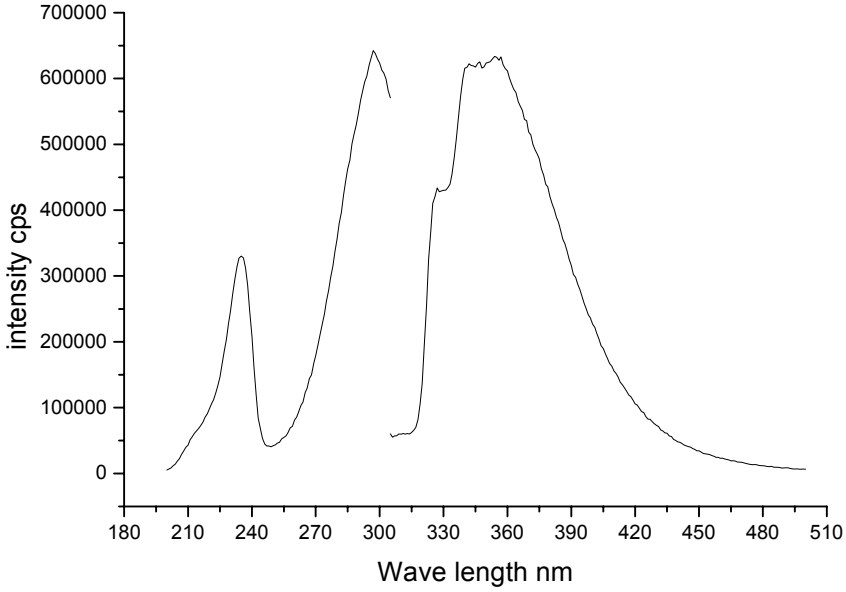

Figure 3.1A. Room temperature excitation and fluorescence spectra of 100 ng/mL 1-OHnap in methanol/water (0.05% v/v)

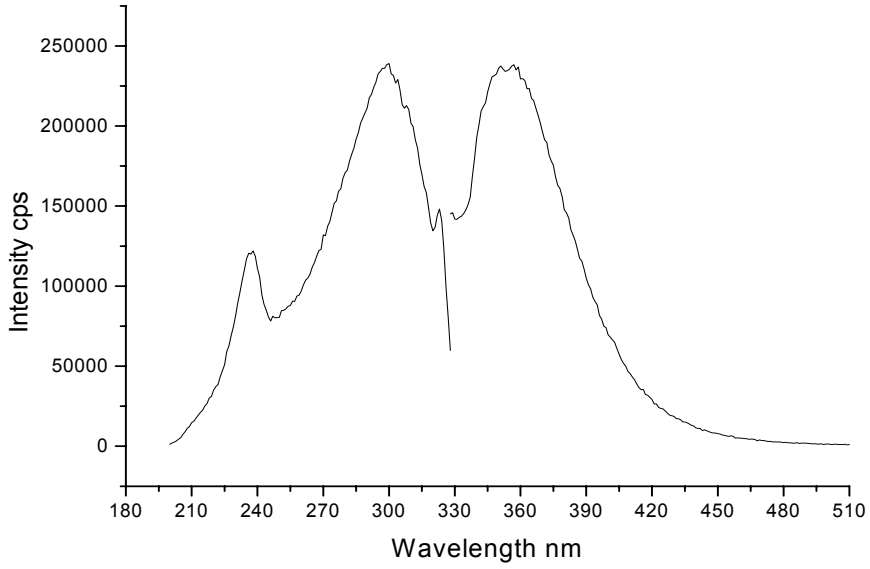

Figure 3.1B. Room temperature excitation and fluorescence spectra of 50 ng/mL 1-OHnap in methanol.

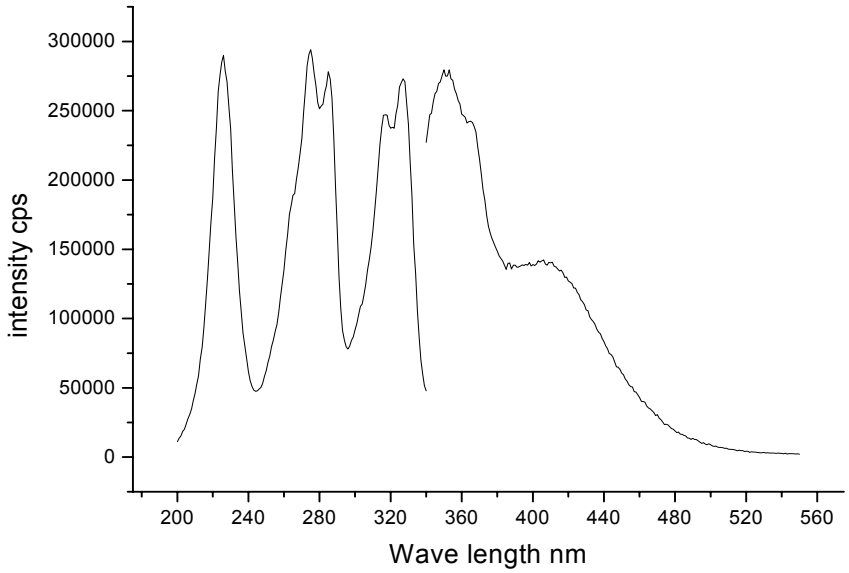

Figure 3.2A. Room temperature excitation and fluorescence spectra of 100 ng/mL 2-OHnap in methanol/water (0.05% v/v)

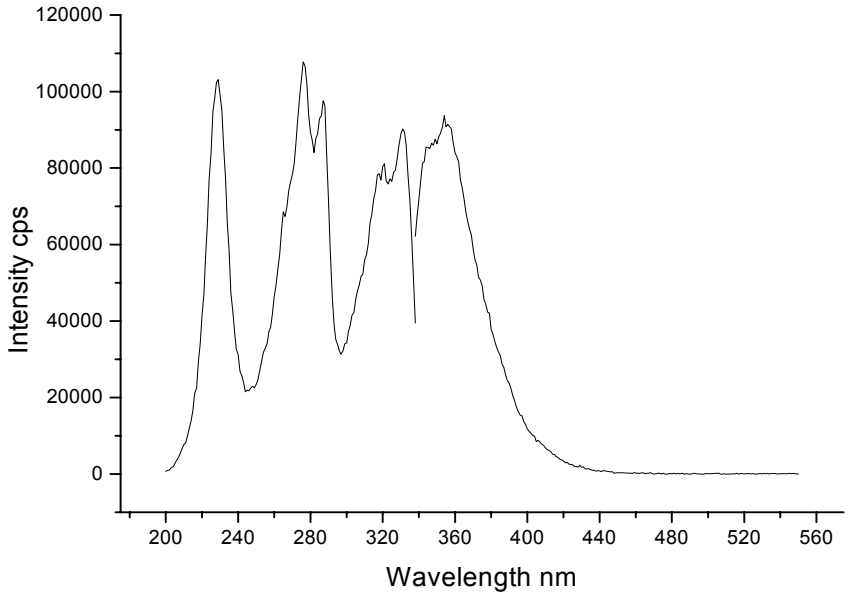

Figure 3.2B. Room temperature excitation and fluorescence spectra of 50 ng/mL 2-OHnap in methanol

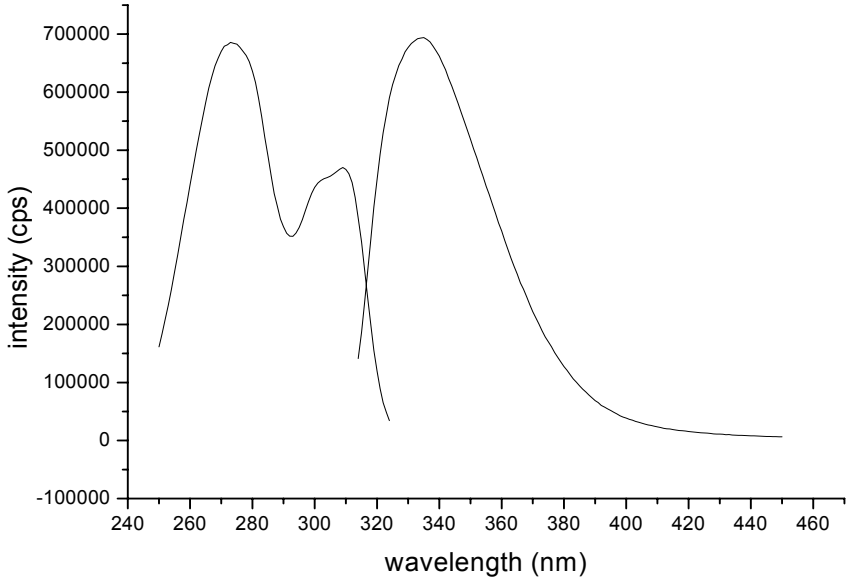

Figure 3.3A. Room temperature excitation and fluorescence spectra of 50 ng/mL 2-OHflu in methanol/water (0.05% v/v)

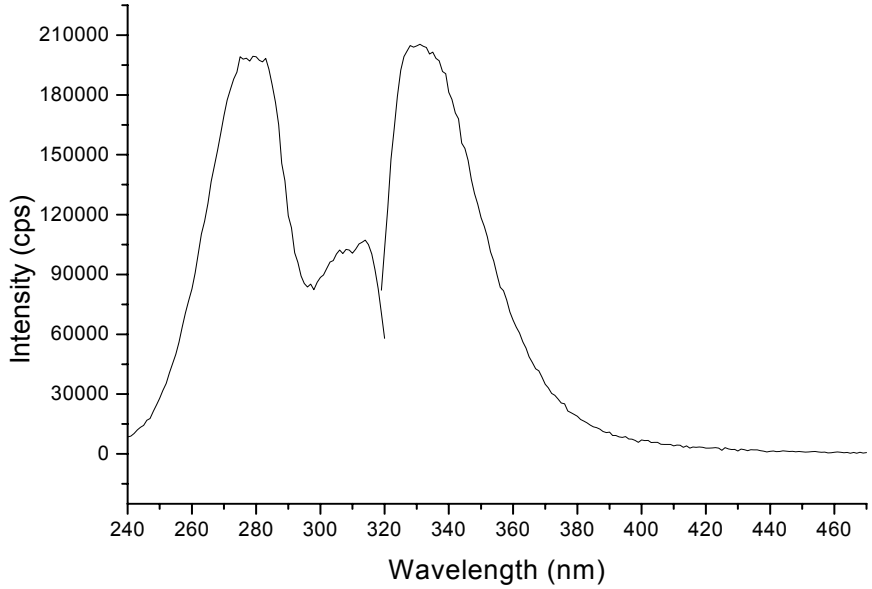

Figure 3.3B. Room temperature excitation and fluorescence spectra of 50 ng/mL 2-OHflu in methanol

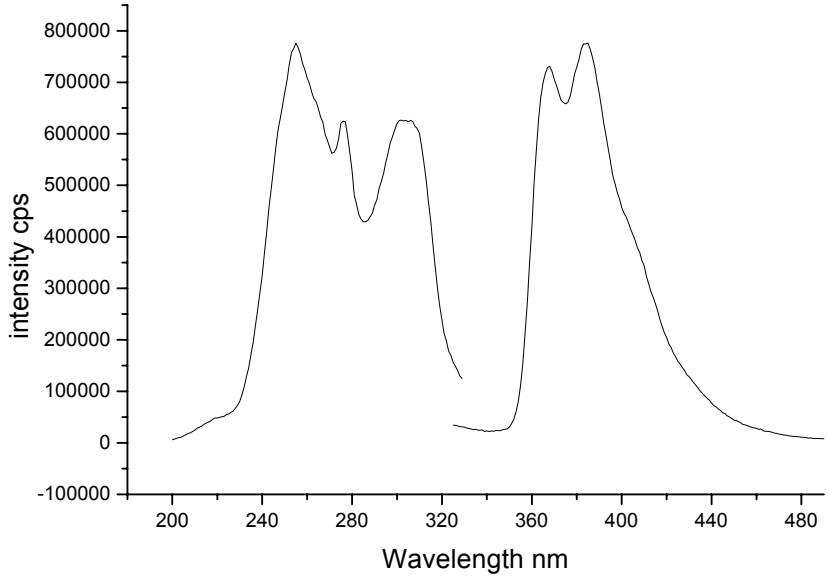

Figure 3.4A. Room temperature excitation and fluorescence spectra of 100 ng/mL 9-OHphe in methanol/water (0.05% v/v)

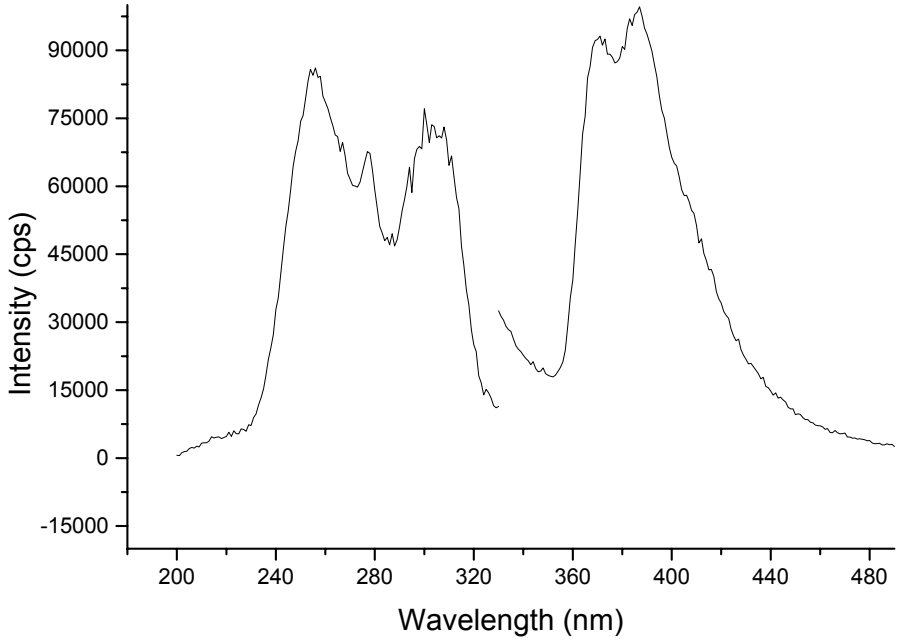

Figure 3.4B. Room temperature excitation and fluorescence spectra of 20 ng/mL 9-OHphe in methanol

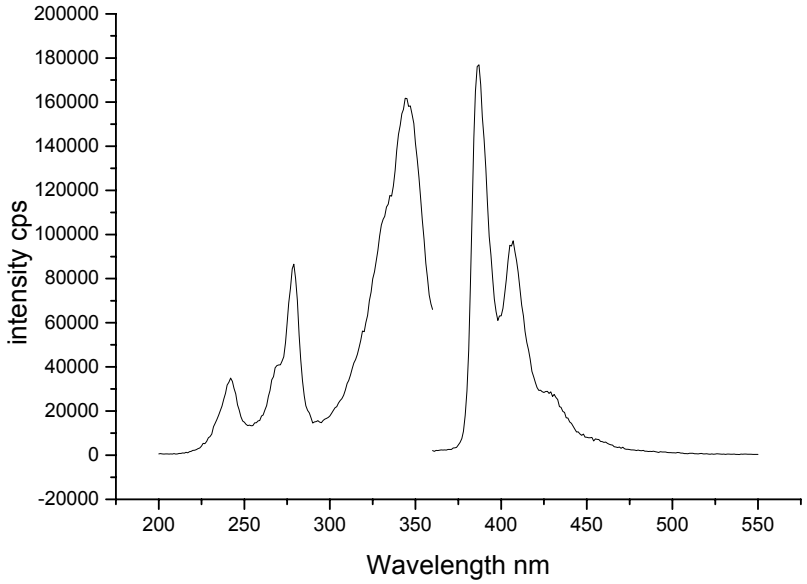

Figure 3.5A. Room temperature excitation and fluorescence spectra of 100 ng/mL 1-OHpyr in methanol/water (0.05% v/v).

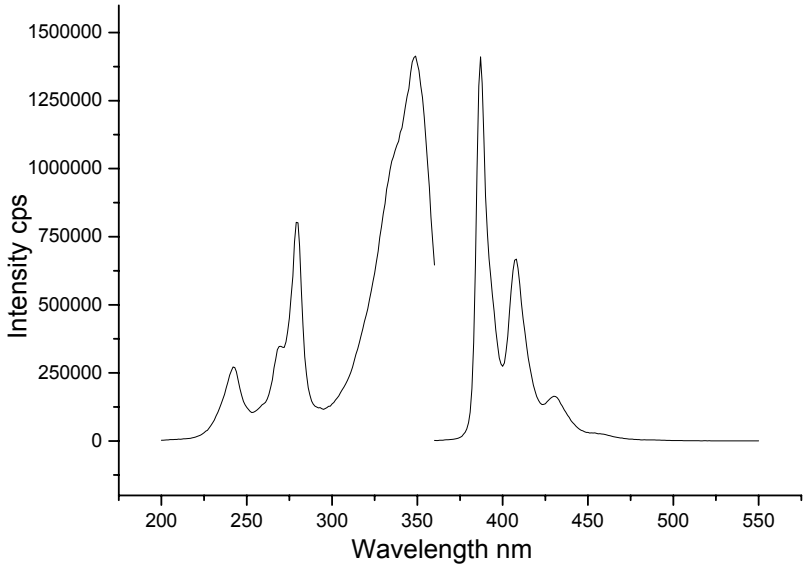

Figure 3.5B. Room temperature excitation and fluorescence spectra of 100 ng/mL 1-OHpyr in methanol.

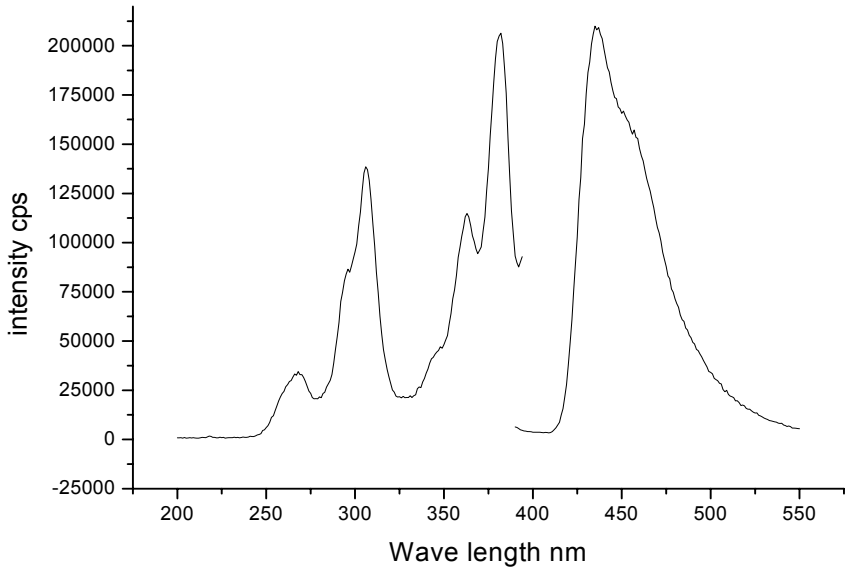

Figure 3.6A. Room temperature excitation and fluorescence spectra of 50 ng/mL 3-OHb[a]p in methanol/water (0.05% v/v).

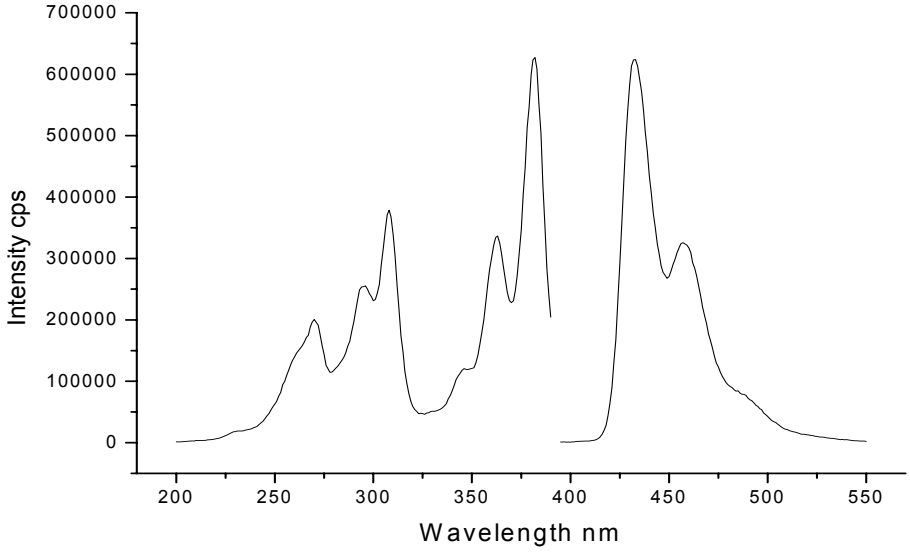

Figure 3.6B. Room temperature excitation and fluorescence spectra of 50 ng/mL 3-OHb[a]p in methanol

Table 3.1. Excitation and Emission Wavelengths[a] of PAHm in water

PAHm	*Excitation Wavelength nm*	*Emission Wavelength nm*
1-OHnap	235s, 297	353
2-OHnap	225, 275, 284s, 316s,327	353, 407s
2-OHflu	273, 309s	334
9-OHphe	254, 275s, 303	367, 384
1-OHpyr	242, 278, 345	386, 405
3-OHb(a)p	269, 304, 363s, 381	435

[a] Table 3.1. Underlined wavelengths indicate the maximum excitation or emission wavelength; s- shoulder wavelength.

Table 3.2 Excitation and Emission Wavelengths of PAHm in methanol.

PAHm	*Excitation Wavelength nm*	*Emission Wavelength nm*
1-OHnap	236s, 299	357
2-OHnap	229, 276, 286s, 331	357
2-OHflu	222s, 278	301s, 328
9-OHphe	254, 275s, 305	367, 385
1-OHpyr	243, 277, 348	387, 407, 430s
3-OHb(a)p	270, 294s, 308, 362s, 382	432, 457s

Table 3.2. Underlined wavelengths indicate the maximum excitation or emission wavelength; s- shoulder wavelength.

Table 3.3 summaries the RTF AFOM of the six metabolites in methanol/water 0.05% v/v. Working solutions were prepared from intermediate stock solutions

(500ng/mL) by serial dilution with methanol-water (0.05% v/v). Fluorescence measurements were made at the maximum excitation and fluorescence wavelength of each compound. Each calibration curve was built with a minimum of five analyte concentrations. For each concentration plotted in the calibration graph, the RTF intensity was the average of at least three determinations taken from three sample aliquots. No efforts were made to experimentally obtain the upper concentration limit of the calibration curve. The main reason was the fact that 50ng/mL and 100ng/mL, i.e. the highest concentrations tested in these studies, are already at the highest concentration ranges of OH-PAH typically found in urine. [3-7] It is important to note, however, that 50ng/mL and 100ng/mL did not surpass the breakdown volume of the SPE device. [43] The equation for the straight line that best fitted the experimental data points was calculated via the least squares method. [44] The correlation coefficients of the calibration curves and the slopes of the log-log-plots were close to unity, indicating a linear relationship between OH-PAH concentration and fluorescence intensity. Within the LDR, the relative standard deviations (RSD) at medium concentrations were lower than 2%. The limits of detection (LOD) were calculated using equation (3):

$$LOD = 3 \times S_B / m \qquad (3)$$

where S_B is the standard deviation of sixteen blank determinations and m is the slope of the calibration curve. [45]

Table 3.3 RTF[f]-Analytical Figures of Merit of PAHm in methanol/water (0.05% v/v)

PAHm	$\lambda_{ex/em}$[a]	*LDR*[b]	*Slope log-log plot*	R^{2}[c]	*LOD*[d]	*LOQ*[e]
1-OHnap	299/357	1.55-100	0.9986	0.9999	0.471	1.553
2-OHnap	331/357	12.1-100	0.9992	0.9999	3.682	12.16
2-OHflu	278/328	1.57-50	0.9861	0.9998	0.478	1.577
9-OHphe	305/367	2.37-100	0.9792	0.9989	0.720	2.376
1-OHpyr	348/387	0.23-50	0.9936	0.9997	0.070	0.231
3-OHb(a)p	381/432	0.31-50	0.9849	0.9933	0.094	0.312

[a] Maximum excitation and emission wavelength in nm.

[b] Linear dynamic range in ng/mL

[c] Correlation coefficient of calibration curve

[d] Limit of detection (ng/mL) calculated from 3 × standard deviation(s_b) of sixteen blank measurements divided by slope(m) of the calibration curve.

[e] Limit of Quantification (ng/mL) is calculated from $10s_b/m$

[f] RTF- Room temperature fluorescence

Figures 3.7 to 3.12 illustrate the calibration curves of the six OH-PAH in methanol. The equations of the straight lines that best fit the experimental data points were calculated via the least squares method. [44]

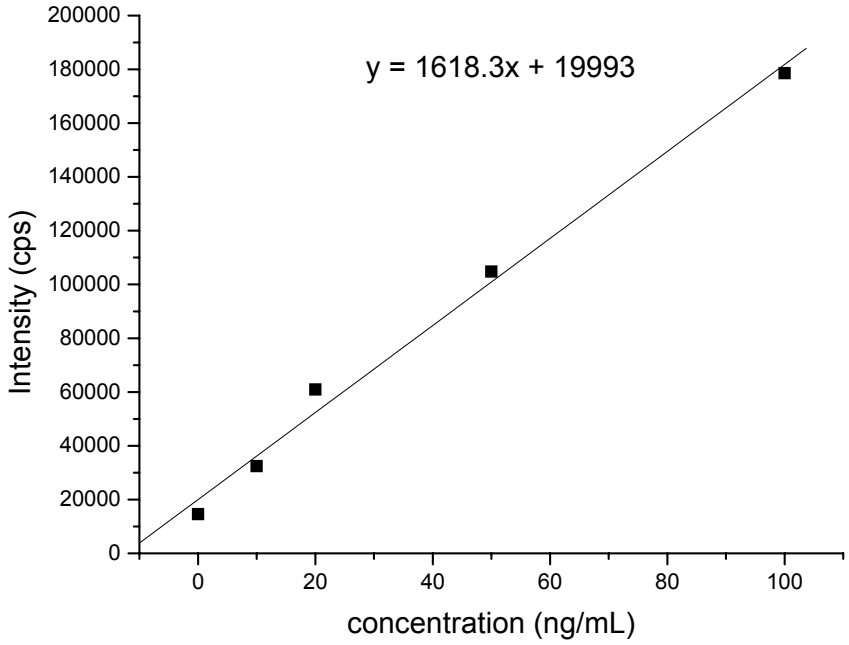

Figure 3.7 RTF-calibration curve of 1-OHnap in methanol

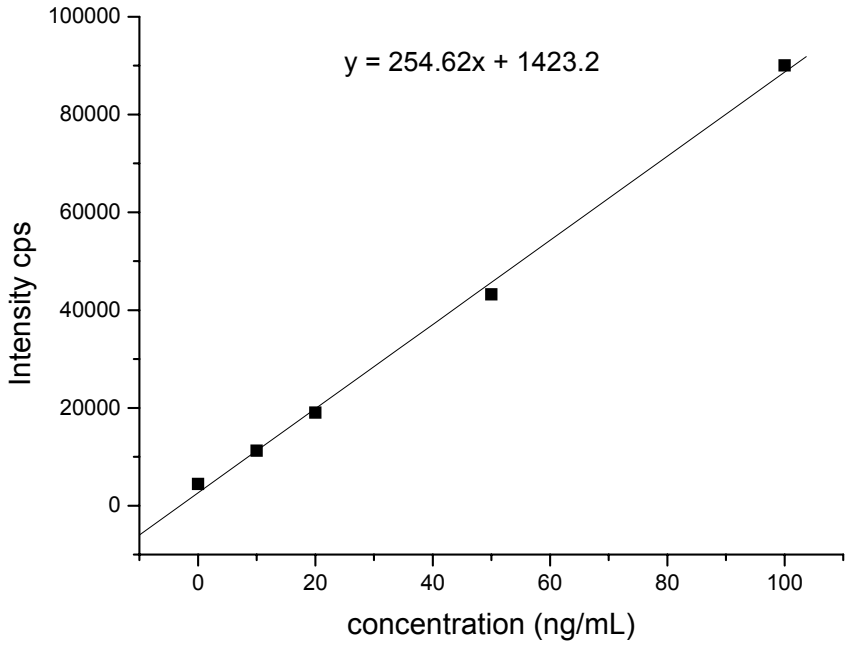

Figure 3.8 RTF-calibration curve of 2-OHnap in methanol

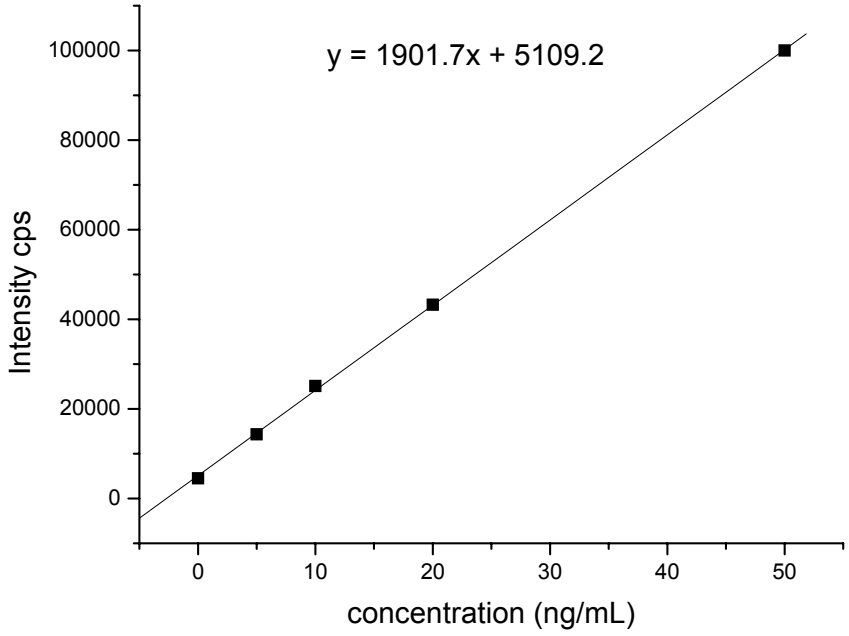

Figure 3.9 RTF-calibration curve of 2-OHflu in methanol

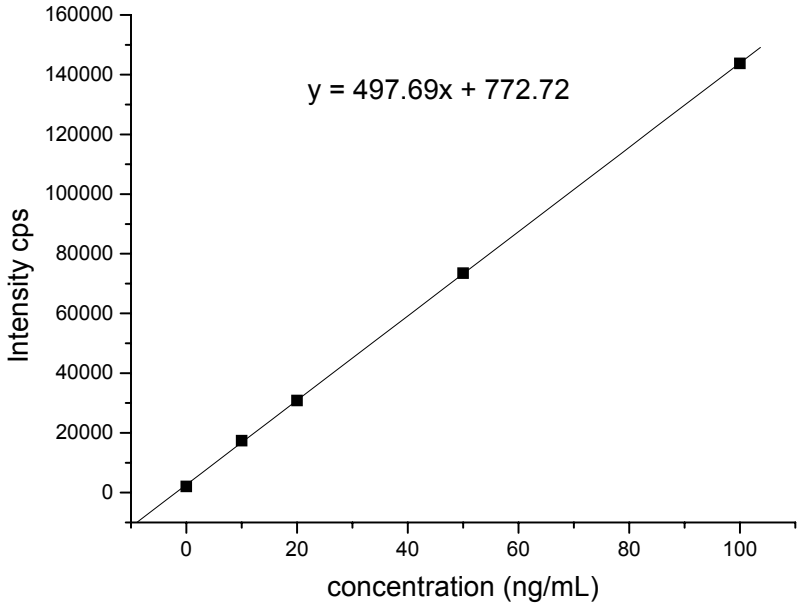

Figure 3.10 RTF-calibration curve of 9-OHphe in methanol

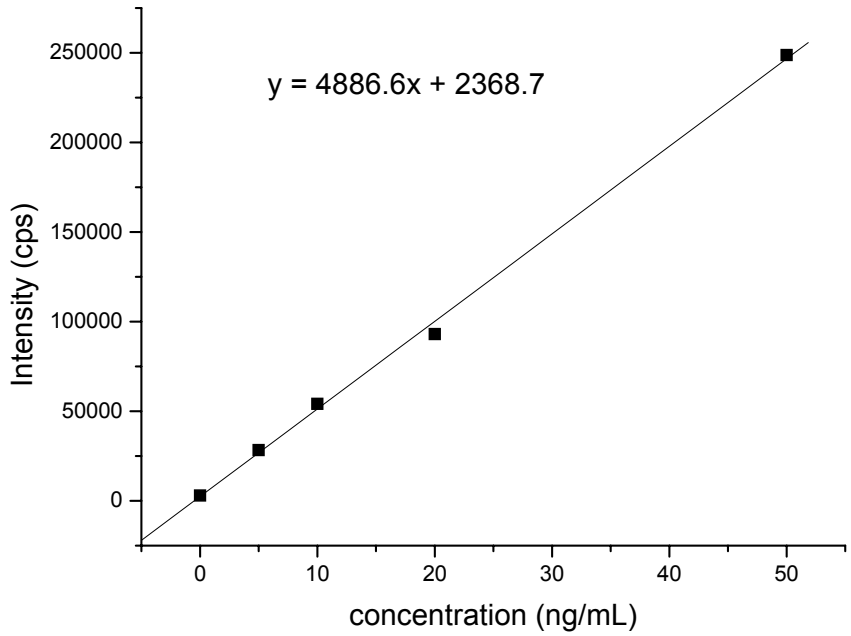

Figure 3.11 RTF-calibration curve of 1-OHpyr in methanol

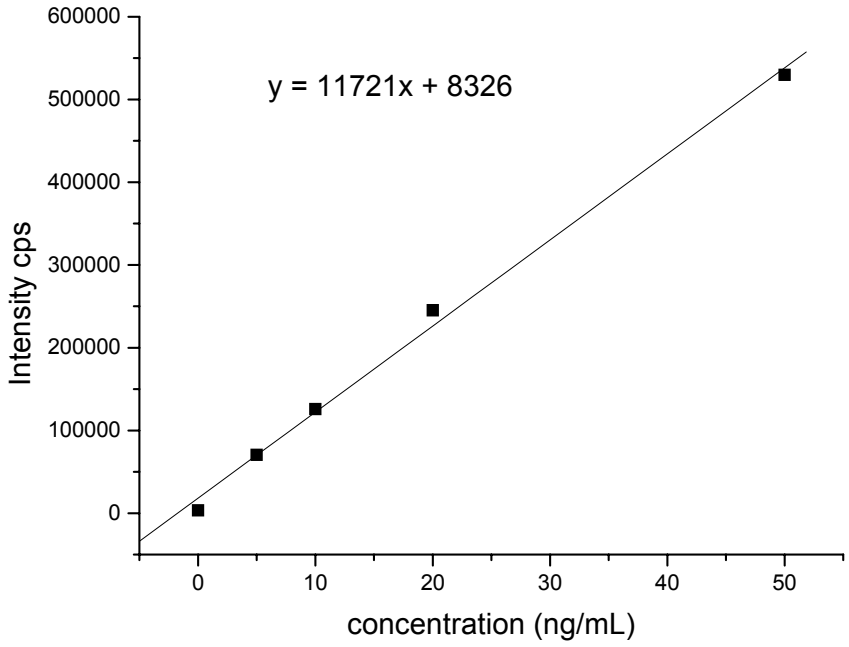

Figure 3.11 RTF-calibration curve of 3-OHb[a]p in methanol

Table 3.4 summaries their AFOM. Working solutions were prepared from intermediate stock solutions (500ng/mL) by serial dilution with methanol. Fluorescence measurements were made at the maximum excitation and fluorescence wavelength of each compound. Each data point in the calibration graph represents the average intensity of three fluorescence measurements taken from three standard aliquots. No attempts were made to experimentally obtain the upper concentration limit of the calibration curve. The upper limit of the LDR in methanol includes the highest concentration of OH-PAH tested in water and, therefore, it is well suited for the purpose at hand. The correlation coefficients of the calibration curves and the slopes of the log-log-plots were close to unity, indicating a linear relationship between OH-PAH concentration and fluorescence intensity. The limits of quantitation (LOQ) were calculated according to the formula: [44]

$$LOQ = 10 \times S_B / m \qquad (4)$$

At this concentration level, the RSD of fluorescence measurements varied between 5 and 7%, allowing us to make precise measurements at low ppb level.

Table 3.4. RTF[f]-Analytical Figures of Merit of PAHm in methanol

PAHm	$\lambda_{ex/em}$[a]	*LDR*[b]	*Slope log-log plot*	R^{2}[c]	*LOD*[d]	*LOQ*[e]
1-OHnap	299/357	1.43-100	0.9933	0.9917	0.431	1.435
2-OHnap	331/357	3.90-100	0.9998	0.9990	1.171	3.899
2-OHflu	278/328	1.58-50	0.9985	0.9997	0.474	1.578
9-OHphe	305/367	1.01-100	0.9999	0.9998	0.304	1.012
1-OHpyr	348/387	0.23-50	0.9960	0.9983	0.068	0.226
3-OHb(a)p	381/432	0.18-50	0.9988	0.9998	0.054	0.180

[a] Maximum excitation and emission wavelength in nm.

[b] Linear dynamic range in ng/mL

[c] Correlation coefficient of calibration curve

[d] Limit of detection (ng/mL) is calculated from 3 × standard deviation(s_b) of sixteen blank measurements divided by slope(m) of the calibration curve.

[e] Limit of Quantification (ng/mL) is calculated from $10s_b/m$

[f] RTF- Room temperature fluorescence

3.2. Optimization of SPE

The concentration factor (CF) in SPE is defined as the ratio between the sample volume (V_S) and the volume of organic solvent (V_E) used in the final eluting step:

$$CF = V_S / V_E \quad (5)$$

For any giving volume of eluting solvent, the best concentration factor is obtained when the sample volume matches the breakthrough volume of the sorbent. This is the path most analysts pursue for the optimization of SPE parameters in environmental analysis of water samples. Larger sample volumes than the breakthrough volume are avoided to prevent analyte loss. Within the context of urine analysis, where the volume of sample is somehow limited, appears to be a general consensus that 10mL is an appropriate urine volume. [3,4]

Our primary objective was then to reduce the volume of eluting solvent. V_E was optimized monitoring the fluorescence of metabolites in the eluting solvent as a function of its volume. The metabolites concentrations were calculated using the equations of the calibration curves in methanol (see Figures 3.7 to 3.12). The % of elution was calculated according to equation 2. All metabolites showed similar eluting profiles to the one depicted for 2-naphthol in Figure 3.13. The best eluting efficiencies were obtained for 3 and 4mL of methanol. Because 3mL of methanol would provide a better CF than 4mL, we adopted 3mL as the optimum volume of eluting solvent for all the remaining extractions.

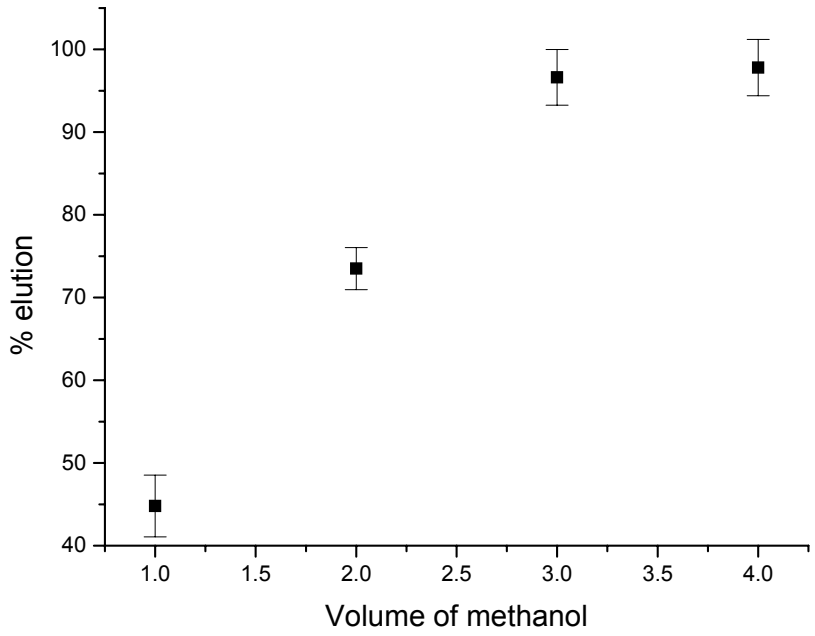

Figure 3.13. Elution profile of 2-OHnap in methanol

The next attempt was to reduce the volume of the eluted solution to the minimum possible volume for RTF measurements. In our case, this volume was 300mL, which is equivalent to the volume of the smallest cuvettes available in our lab. The eluted solution was then evaporated - under a gentle stream of nitrogen gas - to almost dryness and re-dissolved in 1mL of methanol for RTF measurements. The 1mL of solution would allow for three individual measurements of 300μL aliquots. Significant analyte loss was observed in all cases. Following a previously published procedure, [46] 10 μL of dodecane (CH_3-$(CH_2)_{10}$-CH_3) were added to the eluate to prevent metabolite evaporation. An improvement was observed in all cases but the % recoveries were still lower than in the absence of evaporation.

Table 3.5 summaries the figures of merit for the optimized SPE procedure in water samples. The overall efficiency was calculated with equation (6):

Overall efficiency = % retention x % elution (6)

The standard deviations of overall efficiencies (S_{OE}) are based on three repetitions of the entire SPE procedure and were calculated as follows:

$$S_{OE} / OE = [(S_{RE} /RE)^2 + (S_{EL}/EL)^2]^{1/2}$$

Where OE refers to the overall efficiency, RE represents the % retention, EL is the % elution, and S_{RE} and S_{EL} are their respective standard deviations. [47]

Table 3.5. Efficiency of SPE in water sample

PAHm	*% Retention* $\boldsymbol{RE} \pm S_{ret}$ [a]	*% Elution Efficiency* $\boldsymbol{EE} \pm S_{elu}$ [b]	*% Overall Efficiency* $\boldsymbol{OE} \pm S_o$ [c]
1-OHnap	99.41 ± 0.53	98.38 ± 1.44	96.33 ± 1.50
2-OHnap	95.72 ± 0.40	96.85 ± 0.81	92.70 ± 0.93
2-OHflu	99.91 ± 0.10	99.26 ± 1.78	99.17 ± 1.79
9-OHphe	98.82 ± 0.12	91.40 ± 1.79	90.32 ± 1.96
1-OHpyr	99.29 ± 0.23	89.10 ± 1.32	88.46 ± 1.49
3-OHb[a]p	99.03 ± 0.32	99.18 ± 1.44	98.22 ± 1.48

a- % standard deviation of % retention efficiency

b- % standard deviation of % elution efficiency

c- % standard deviation of % overall efficiency

Table 3.6 summaries the same figures of merit for OH-PAH extracted from urine samples. The last column in this table presents the statistical comparison of the overall efficiencies to those obtained from aqueous samples (see values in Table 3.5). Within a confidence interval of 95% and 3 determinations, the overall efficiencies were statistically equivalent in all cases. This fact demonstrates that the matrix composition of the urine sample does not interfere with the SPE procedure.

Table 3.6. Efficiency of SPE in urine sample

PAHm	*% Retention* ***RE*** $\pm S_{ret}$ [a]	*% Elution Efficiency* ***EE*** $\pm S_{elu}$ [b]	*% Overall Efficiency* ***OE*** $\pm S_o$ [c]	t_{exp} [d]
1-OHnap	96.57 ± 1.12	99.01 ± 1.35	95.61 ± 1.78	0.542
2-OHnap	96.66 ± 2.08	99.96 ± 2.59	96.62 ± 3.36	1.023
2-OHflu	99.79 ± 0.28	95.74 ± 2.88	95.53 ± 3.02	1.838
9-OHphe	99.27 ± 0.30	88.57 ± 1.31	87.92 ± 1.51	1.724
1-OHpyr	99.55 ± 0.38	88.51 ± 0.95	88.11 ± 1.13	0.331
3-OHb[a]p	99.63 ± 0.12	99.80 ± 1.04	99.43 ± 1.05	1.179

a- % standard deviation of % retention efficiency

b- % standard deviation of % elution efficiency

c- % standard deviation of % overall efficiency

d- t_{exp} – t value calculated for experimental measurements

t_{tab} – tabulated 't' value for degrees of freedom is 2.78.

3.3. SPE-RTF Analytical Figures of Merit for the Analysis of OH-PAH in Urine Samples

Table 3.7 summaries the AFOM for OH-PAH metabolites in urine. 10mL of urine samples were individually spiked with standard solutions of known concentrations of metabolites and submitted to the entire SPE-RTF procedure. Blank signals were obtained from non-spiked urine samples submitted to the same experimental procedure as the spiked samples. Comparison of LOD to those in Table 3.3 shows good agreement to our expectations. The concentration factor of SPE ($CF = V_S / V_E = 10mL / 3mL = 3.3$) provides an improvement of ~ 3x in the LOD.

Table 3.7. SPE-RTF[f] Analytical Figures of Merit of OH-PAH in urine.

PAHm	$\lambda_{ex/em}$ [a]	*LDR*[b]	*Slope log-log plot*	R^2[c]	*LOD*[d]	*LOQ*[e]
1-OHnap	299/357	0.57-100	0.9928	0.9996	0.173	0.576
2-OHnap	331/357	2.08-100	0.9957	0.9989	0.625	2.081
2-OHflu	278/328	0.52-50	0.9888	0.9986	0.156	0.519
9-OHphe	305/367	0.45-100	0.9990	0.9999	0.136	0.452
1-OHpyr	348/387	0.11-50	0.9994	0.9971	0.033	0.109
3-OHb[a]p	381/432	0.04-50	0.9923	0.9782	0.014	0.046

[a] Maximum excitation and emission wavelength in nm.

[b] Linear dynamic range in ng/mL

[c] Correlation coefficient of calibration curve

[d] Limit of detection (ng/mL) is calculated from 3 × standard deviation(s_b) of sixteen blank measurements divided by slope(m) of the calibration curve.

[e] Limit of Quantification (ng/mL) is calculated from $10s_b/m$

[f] SLE-RTF- Solid liquid extraction room temperature fluorescence.

According to equation 3, the slope of the calibration curve and the standard deviation of the blank signal are the two parameters that affect LOD values. Table 3.8 compares these two figures for RTF and SPE-RTF. The slopes obtained via SPE-RTF are approximately 3x higher than those obtained via RTF. The steeper slopes are in excellent agreement with the concentration factors of SPE. Because the standard deviations of the blank signals are approximately the same for all OH-PAH, the 3x improvement in LOD can be mostly attributed to the enrichment factor obtained with SPE. Larger sample volumes would certainly improve LOD.

Table 3.8. Comparison of Slopes and Standard deviation between RTF and SPE-RTF

	Slope		*Standard deviation*	
PAHm	RTF	SPE-RTF	RTF	SPE-RTF
1-OHnap	1618.3	5432.3	232.8	313.1
2-OHnap	254.62	864.93	99.4	180.4
2-OHflu	1901.7	5310.3	277.4	300.2
9-OHphe	496.6	1413.6	50.58	64.28
1-OHpyr	4886.6	15494	112.3	174.1
3-OHb[a]p	11721	49607	212.1	237.3

Figure 3.14 compares the excitation and fluorescence spectrum of pure methanol to those recorded from 3mL of methanol eluted from SPE cartridges previously used to extract blank samples consisting 10mL of water-methanol (0.05% v/v) solution and 10mL of non-spiked urine sample. The excitation and emission wavelengths used to

record the spectra were the maxima for 2-naphthol. The same spectral behavior was observed at all the other excitation/emission maxima of OH-PAH. This is a strong indication that the main contribution to the background signal comes from fluorescence impurities present in the SPE cartridge.

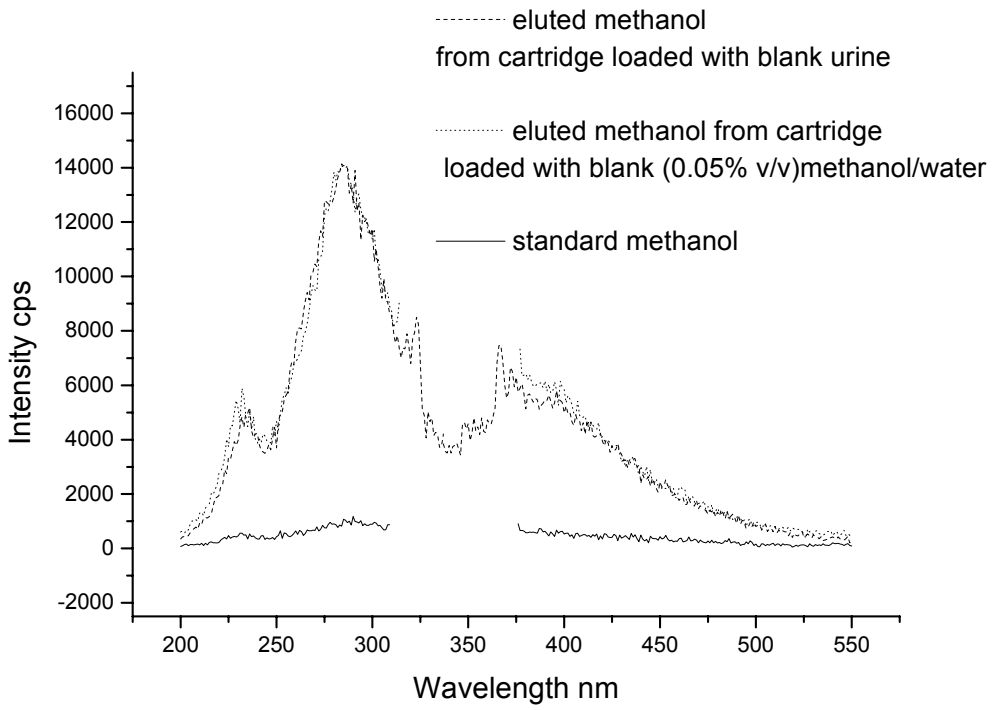

Figure 3.14. Comparison of excitation and fluorescence spectra of pure methanol, eluted methanol from cartridge loaded with blank (0.05% v/v) methanol/water and eluted methanol from cartridge loaded with unspiked urine.

Reducing the blank signal usually leads to smaller standard deviations and, therefore, better LOD. One possibility that was not pursued is to remove the fluorescence impurities from the cartridge. This could be accomplished by flushing methanol through the cartridge prior to SPE.

3.4. Analysis of Synthetic Mixtures of OH-PAH in Urine Samples via SPE-RTF

Close examination of figures 3.1(B) to 3.6(B) show strong overlapping of excitation and fluorescence spectra. Potential overlapping from co-existing metabolites has prevented the direct determination of target OH-PAH without previous chromatographic separation. The combination of multidimensional formats - such as EEM - to multi-way spectral de-convolution methods – such as Parallel Factor Analysis (PARAFAC) - has shown promise for the simultaneous determination of parent PAH in matrixes of unknown composition. [48,49] This algorithm carries with it the second order advantage, which refers to the ability of simultaneously strip multiple pure spectral profiles from multi-way data even in the presence of unknown, un-calibrated interference. [50,51] Other methodologies - based on the use of latent variables - do also exist for processing EEM. [52-54]

The combination of unfolded Partial Least-Squares (U-PLS) to Residual Bi-Linearization (RBL) was recently explored as a valuable alternative for processing EEM while preserving the second order advantage. U-PLS/RBL provided accurate determination of the antibiotic tetracycline and the anti-inflammatory salicylate in the presence of strong matrix interference from human sera. [55,56] The work presented here further explores the potential of this approach for the direct determination of the six studied OH-PAH. EEM were recorded in our lab, saved in ASCII format and sent via e-mail to Dr. H. C. Goicoechea (Universidad Nacional del Litoral, Santa Fe, Argentina) for chemometric analysis. The software for U-PLS/RBL analysis was developed in house by Oliveri et al. [57]

This algorithm comprises a first calibration step in which concentration information is employed including data exclusively from standards of known composition. [58] The I calibration data matrices $\mathbf{X}_{c,i}$ (size $J \times K$, where J and K are the number of channels in each dimension) are vectorized (unfolded) and used to calibrate the U-PLS model and the vector of calibration concentrations $\mathbf{y}$ ($N_c \times 1$, where N_c is the number of calibrated analytes). This provides a set of loadings $\mathbf{P}$ and weight loadings $\mathbf{W}$ (both of size $JK \times A$, where A is the number of latent factors), as well as regression coefficients $\mathbf{v}$ (size $A \times 1$). Techniques such as leave-one-out cross-validation allow for the acquisition of the parameter A. [59] If no unexpected interferences occur in the test sample, $\mathbf{v}$ can be employed to estimate the analyte concentration with the following equation:

$$y_u = \mathbf{t}_u^T \mathbf{v} \tag{8}$$

where $\mathbf{t}_u$ is the test sample score, which is obtained by projection of the (unfolded) data for the test sample $\mathbf{X}_u$ onto the space of the A latent factors:

$$\mathbf{t}_u = (\mathbf{W}^T \mathbf{P})^{-1} \mathbf{W}^T \mathrm{vec}(\mathbf{X}_u) \tag{9}$$

When unexpected constituents occur in $\mathbf{X}_u$, then the sample scores given by equation (9) are not suitable for analyte prediction using equation (8). In this case, the residuals of the U-PLS prediction step [s_p, see equation (10)] will be abnormally large in comparison with the typical instrumental noise. This is usually assessed by replicate measurements:

$$s_p = \| \mathbf{e}_p \| / (JK–A)^{1/2} = \| \mathrm{vec}(\mathbf{X}_u) – \mathbf{P} (\mathbf{W}^T \mathbf{P})^{-1} \mathbf{W}^T \mathrm{vec}(\mathbf{X}_u) \| / (JK–A)^{1/2}$$
$$= \| \mathrm{vec}(\mathbf{X}_u) – \mathbf{P}\, \mathbf{t}_u \| / (JK–A)^{1/2} \tag{10}$$

where $\| \cdot \|$ indicates the Euclidean norm.

If unexpected constituents occur in the test sample, the situation can be handled by a separate procedure called RBL. This procedure is based on singular value decomposition (SVD) modeling of the interferent effects. It aims at minimizing the norm of the residual vector $\mathbf{e}_u$, computed while fitting the sample data to the sum of the relevant contributions to the sample signal. For a single interferent:

$$\text{vec}(\mathbf{X}_u) = \mathbf{P}\,\mathbf{t}_u + \text{vec}[g_{int}\,\mathbf{b}_{int}\,(\mathbf{c}_{int})^T] + \mathbf{e}_u \qquad (11)$$

where $\mathbf{b}_{int}$ and $\mathbf{c}_{int}$ are the left and right eigenvectors of $\mathbf{E}_p$ and g_{int} is a scaling factor:

$$(g_{int}, \mathbf{b}_{int}, \mathbf{c}_{int}) = \text{SVD}_1(\mathbf{E}_p) \qquad (12)$$

where $\mathbf{E}_p$ is the $J \times K$ matrix obtained after reshaping the $JK \times 1$ $\mathbf{e}_p$ vector of equation (10), and SVD_1 indicates taking the first principal component.

During this RBL procedure, $\mathbf{P}$ is kept constant at the calibration values and $\mathbf{t}_u$ is varied until $\| \mathbf{e}_u \|$ is minimized. The minimization can be carried out using a Gauss-Newton (GN) procedure starting with $\mathbf{t}_u$ from equation (10). Once $\| \mathbf{e}_u \|$ is minimized in equation (11), analyte concentrations are obtained by introducing the final $\mathbf{t}_u$ vector in equation (8).

The number of unexpected constituents N_{unx} can be assessed by comparing the final residuals s_u with the instrumental noise level:

$$s_u = \| \mathbf{e}_u \| / [JK - (N_c + N_{unx})]^{1/2} \qquad (13)$$

where $\mathbf{e}_u$ is from equation (11). A plot of s_u computed for trial number of components will show decreasing values, starting at s_p when the number of components is equal to A,

i.e. the number of latent variables used to describe the calibration data, until it stabilizes at a value compatible with the experimental noise, allowing to locate the correct number of components. It should be noted that for $N_{unx} > 1$, the profiles provided by the SVD analysis of $\mathbf{E}_p$ unfortunately no longer resemble the true interferent profiles. This is due to the fact that the principal components are restricted to be orthonormal.

3.4.1. Calibration, Validation Samples and Synthetic Samples

Table 3.9 summaries the composition of both calibration and validation sets selected for these studies using fractional factorial design. Nine mixtures were selected for each purpose containing various concentrations of the six metabolites. The relatively high concentrations of OH-PAH metabolites were purposely selected to obtain true spectral fingerprints with insignificant contributions from fluorescence background and instrumental noise. All synthetic mixtures were prepared in methanol previously flushed through an SPE cartridge disk. The same procedure was used for blank samples to account for background subtraction of fluorescence impurities. EEM were collected with a commercial spectrofluorimeter. Excitation wavelengths were varied at 5nm steps from 200 – 320nm. Sample excitation was carried out from longer t shorter wavelengths to reduce of photo-degradation due to extensive sample excitation. Emission spectra were collected at each excitation wavelength by scanning the emission monochromator from 320 – 550nm. Background subtracted EEM are shown in Appendix A.

Table 3.9. Composition of the calibration and validation set obtained with fractional factorial design.

Sample[a]	1-OHnap (ng/mL)	2-OHnap (ng/mL)	1-OHpyr (ng/mL)	3-OHb[a]p (ng/mL)	2-OHflu (ng/mL)	9-OHphe (ng/mL)
S1	250	250	250	250	250	250
S2	250	0	0	500	125	500
S3	0	0	500	125	500	250
S4	0	500	125	500	250	125
S5	500	125	500	250	125	125
S6	125	500	250	125	125	375
S7	500	250	125	125	375	500
S8	250	125	125	375	500	375
S9	125	125	375	500	375	250
V1	350	300	400	300	350	400
V2	350	60	400	120	350	90
V3	21 3	180	250	210	225	245
V4	75	300	400	120	100	400
V5	75	300	100	120	350	90
V6	75	60	400	300	100	90
V7	350	300	100	300	100	90
V8	75	60	100	300	350	400
V9	350	60	100	120	100	400

[a] S = sample; V = validation.

3.4.2. Optimization of the U-PLS/RBL Model

The number of calibration latent variables for each analyte was estimated by resorting to the well known cross-validation method [60] Table 3.10 shows the spectral regions used for each analyte, the number of latent variables and other pertinent parameters obtained during the calibration process. The spectral regions used in the modelling were selected to increment the selectivity towards each metabolite. The number of factors agrees with the number of metabolites in the calibration samples. The root mean square of error for cross-validation (RMSECV) and the relative error of prediction for the calibration samples (REP%) indicate a reasonable predictive ability for a relatively complex system. Bases on the RMSECV and REP% values, the best

predicting ability should be expected for 3-OHb[a]p and 2-OHflu while the worst results should be expected for 1-OHnap and 2-OHnap

Table 3.10. Parameters Used for the Optimization of the U-PLS/RBL model

Parameter	*1-OHnap*	*2-OHnap*	*1-OHpyr*	*3-OHbap*	*2-OHflu*	*9-OHphe*
Emission (nm)	320–340	330–400	380–440	400–520	320–400	360–445
Excitation (nm)	220–320	220–250	240–320	200–320	240–320	235–320
Factors	6	6	6	6	6	6
RMSECV (ng/mL)	33.1	31.1	13.0	6.7	18.2	26.5
REP(%)	12.2	13.2	8.5	2.2	6.2	8.6

Table 3.11 summaries the prediction values for the nine validation samples presented in Table 3.10. Keeping in mind that 100% is the recovery that would provide the best accuracy of analysis; the closest results to the optimum value were obtained for 3-OHb[a]p and 2-OHflu while the furthest were obtained for 1-OHnap, 2-OHnap and 1-OHpyr. These results are in good agreement with the predicted expectations in Table 3.10.

Table 3.11. Prediction Values for Validation Samples in Table 3.10.

Sample	1-OHnap			2-OHnap			1-OHpyr		
	Nom.[a] (ng/ml)	Pred.[b] (ng/ml)	Recov.[c] (%)	Nom.[a] (ng/ml)	Pred.[b] (ng/ml)	Recov.[c] (%)	Nom.[a] (ng/ml)	Pred.[b] (ng/ml)	Recov.[c] (%)
1	350	394	112.6	300	292	97.3	400	380	95.0
2	350	383	109.4	60	77	161.7	400	431	107.8
3	213	213	100.0	180	191	106.1	250	248	99.2
4	75	89	118.7	300	324	114.7	400	426	106.5
5	75	88	117.3	300	290	96.7	100	121	121.0
6	75	94	125.3	60	78	163.3	400	440	110.0
7	350	388	110.9	300	334	111.3	100	104	104.0
8	75	64	85.3	60	76	143.3	100	105	105.0
9	350	322	92.0	60	55	91.7	100	107	107.0
Average			107.9			110.7			106.2
SD			13.1			14.6			7.2
Sample	3-OHbap			2-OHflu			9-OHphe		
	Nom.[a] (ng/ml)	Pred.[b] (ng/ml)	Recov.[c] (%)	Nom.[a] (ng/ml)	Pred.[b] (ng/ml)	Recov.[c] (%)	Nom.[a] (ng/ml)	Pred.[b] (ng/ml)	Recov.[c] (%)
1	300	288	96.0	350	361	103.1	400	404	101.0
2	120	113	94.2	350	340	97.1	90	78	86.7
3	210	212	101.0	225	241	107.1	245	203	82.9
4	120	125	104.2	100	89	89.0	400	388	97.0
5	120	111	92.5	350	310	88.6	90	75	83.3
6	300	315	105.0	100	95	95.0	90	82	91.1
7	300	320	106.7	100	115	115.0	90	105	116.7
8	300	321	107.0	350	353	100.9	400	384	96.0
9	120	117	97.5	100	113	113.0	400	396	99.0
Average			100.4			101.0			94.8
SD			5.6			9.6			10.6

[a] Nom. = Actual metabolite concentration. [b] Pred. = Predicted metabolite concentration. [c]

Recov. = Recovery = [Pred. / Nom.] x 100.

It should be noted that recovery values in Table 3.11 were calculated with equation 8, i.e. in the absence of unexpected interferences and without the implementation of RBL. To account for the presence of unexpected components (N_{unx}) in the urine sample, one should consider equation 13. Figure 3.15 shows the variation of prediction residuals s_u as a function of trial values of N_{unx} for 1-OHnap in one of the analyzed urine samples. Because the prediction residuals s_u becomes equivalent to the instrumental noise at approximately 5000 counts.s^{-1}, $N_{unx} = 2$ appears to be the corresponding correct choice. The same number of unexpected components was used for all the metabolites in all the analyzed urine samples.

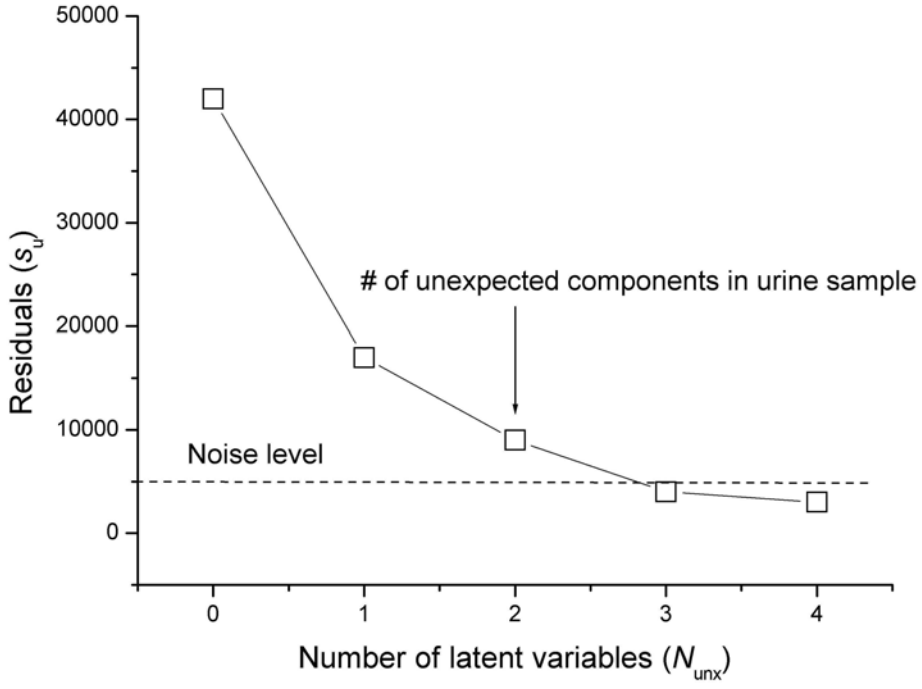

Figure 3.15. Behaviour of Prediction Residuals (Su) for 1-OHnap as a function of unexpected components (N_{unx}) in the urine sample

Table 3.12 summaries the results obtained via SPE-RTF and U-PLS/RBL for three urine samples spiked with meaningful toxicological concentrations of OH-PAH. The obtained results are certainly satisfactory, mainly if one thinks in terms of screening methodology.

Table 3.12. Comparison of Spiked (Spkd.) and Predicted Metabolite Concentrations (ng/mL) in Urine Samples via SPE-RTF and U-PLS/RBL.

[a] Average values correspond to three determinations carried out via the entire SPE-RTF procedure.

Sample	1-OHnap		2-OHnap		1-OHpyr	
	Spkd.	Predicted[a]	Spkd.	Predicted	Spkd.	Predicted[a]
1	40	40.8 ± 4.9	20	19.2 ± 2.5	10	10.4 ± 0.7
2	20	19.1 ± 2.3	40	44.6 ± 5.8	5	8 ± 0.6
3	10	10.8 ± 1.3	5	7 ± 0.9	10	11.5 ± 0.8
	3-OHb[a]p		2-OHflu		9-OHphe	
	Spkd.	Predicted[a]	Spkd.	Predicted[a]	Spkd.	Predicted[a]
1	5	7 ± 0.4	2	1.7 ± 0.2	1	1.08 ± 0.12
2	1	0.84 ± 0.05	10	9.2 ± 0.8	2	1.7 ± 0.19
3	2	2.2 ± 0.1	40	45.3 ± 4.1	20	18.7 ± 2.1

3.5. Low Temperature Fluorescence Characteristics of OH-PAH in "Shipol'skii Matrixes"

The combination of SPE-RTF to U-PLS/RBL is still in its infancy. Further studies with matrixes of higher complexity are needed to evaluate the full analytical potential of this approach for the purpose the hand. The main drawback our studies revealed was the time consuming step of acquiring EEM for calibration and validation purposes. This shortcoming could have been avoided with the implementation of an EEM fluorimeter, such as the one previously described in the literature for the analysis of parent PAH in environmental samples. [60,61] The main components of the reported instrument consist on a continuous wave, 75W xenon lamp, excitation and emission spectrographs and a low- resolution imaging charge coupled device. The main drawbacks of this instrument are the lack of time-resolution capability and the strong interference of Rayleigh scattering. The contribution of the latter to EEM is minimized with the application of a mathematical algorithm to collected data.

The studies presented here build upon significant improvements we have introduced recently to Shpol'skii Spectroscopy. The basis of our approach, which we have named Laser Excited Time-Resolved Shpol'skii Spectrometry (LETRSS), has been previously described towards the analysis of parent PAH in environmental samples. [64-72] The complications of traditional methodology for 77K and 4.2K measurements are avoided by using a bifurcated fiber-optic probe that delivers the excitation light directly into the frozen matrix. This approach retains the simplicity of dunking the sample into the liquid cryogen for fast and reproducible freezing, eliminates all interfaces that could scatter exciting light into the detection system, and also eliminates the need for an optical Dewar and/or helium cryostat. Another significant contribution is the introduction of

novel instrumentation to efficiently collect multidimensional data formats during the lifetime decays of fluorescence (nanoseconds to microseconds) and phosphorescence (milliseconds to seconds) emission. [73, 74] Our instrument takes advantage of the full dimensionality of luminescence spectroscopy combining spectral and lifetime information in multidimensional formats known as wavelength time matrices (WTM) and time-resolved excitation-emission matrices (TREEM). The raw data of such formats provide at least five qualitative parameters for compound determination, namely one excitation, fluorescence and phosphorescence wavelengths and two lifetimes. WTM report on spectral peak purity for selective and accurate determination of target PAH. TREEM give the analyst the opportunity to select the best time window for minimum (or even none) spectral overlapping in highly complex matrixes.

As previously discussed, guest-host compatibility issues have hampered the analysis of OH-PAH via Shpol'skii spectroscopy. The presence of hetero-atoms in their molecular structure limits their solubility in the frozen matrix (usually an n-alkane) and broadens their fluorescence spectra. Direct "fingerprint identification" is no longer possible as closely related isomers show very similar spectra. Here, we present a simple solution to this problem by using an alcohol of appropriate molecular length as the host in the frozen matrix. To the extent of our literature search, this is the first report on this attempt to improve the spectral resolution of PAH metabolites in Shpol'skii matrixes. The OH-PAH used as model compounds are 1-OHpyr, 9-OHphe, 2-OHflu and 3-OHb[a]p.

3.5.1. Choosing the alcohol of appropriate length as Shpol'skii Matrix

A criteria often employed for solvent selection in Shpol'skii spectroscopy matches the length of the solvent molecule to the effective length of the PAH. Based on this criterion, our initial selection included 1-hexanol for 1-OHpyr, 9-OHphe, 1-heptanol for 2-OHflu and 1-octanol for 3-OHb[a]p. Measurements were carried out at 77K with a commercial spectrofluorimeter. Although subsequent studies included various positional isomers for each metabolite, the best spectral resolution was obtained – in all cases - with the alcohol carrying the hydroxyl group in the first carbon atom. Figures 3.16 to 3.19 show the 77K excitation and fluorescence of the studied metabolites in their respective alcohols. Excitation and fluorescence spectra were obtained with 2nm band-pass. No attempts were made to optimize the excitation and emission slits for best spectral resolution or to correct spectra for instrumental response.

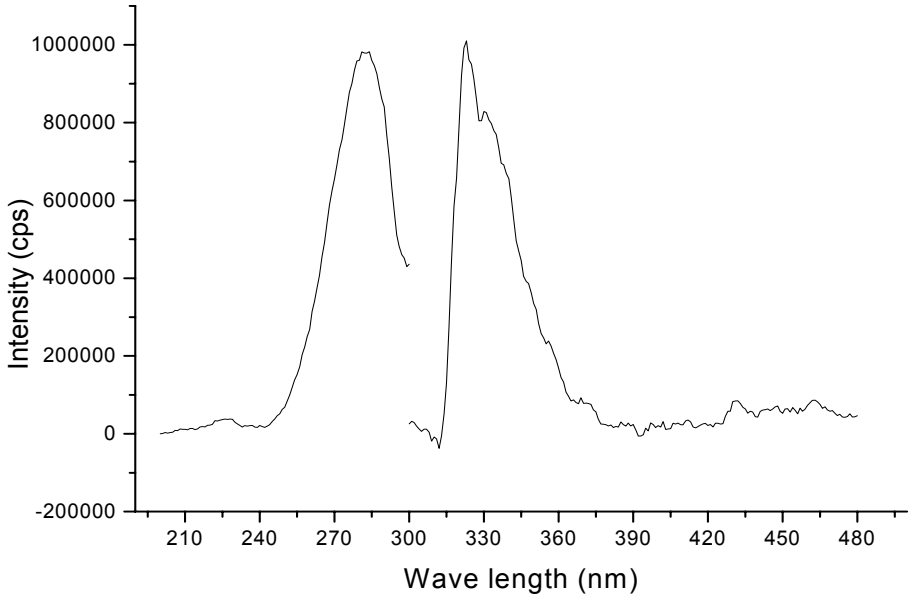

Figure 3.16 Excitation and fluorescence spectra of 50 ng/mL 2-OHflu in 1-heptanol at 77K

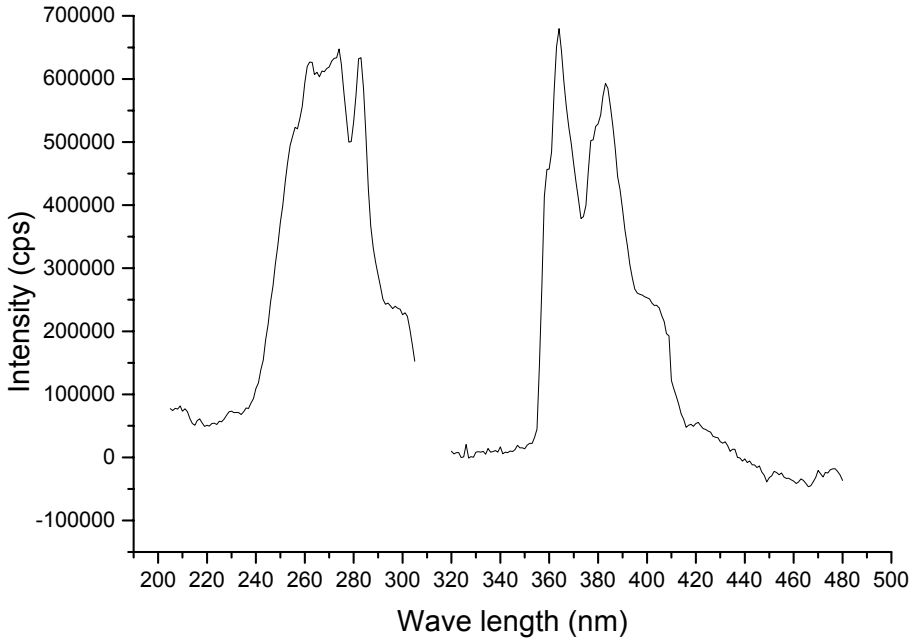

Figure 3.17 Excitation and fluorescence spectra of 50 ng/mL 9-OHphe in 1-heptanol at 77K

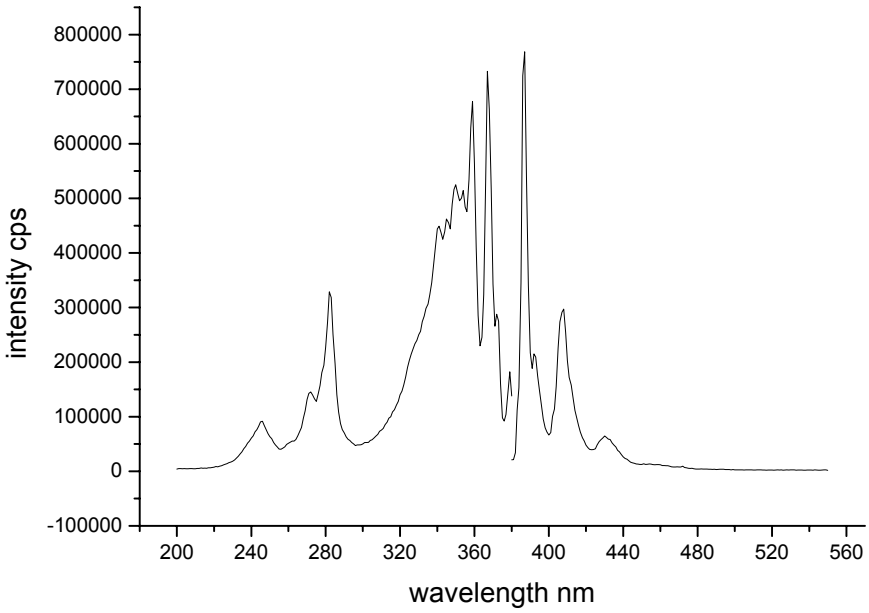

Figure 3.18 Excitation and fluorescence spectra of 20 ng/mL 1-OHpyr in 1-hexanol at 77K

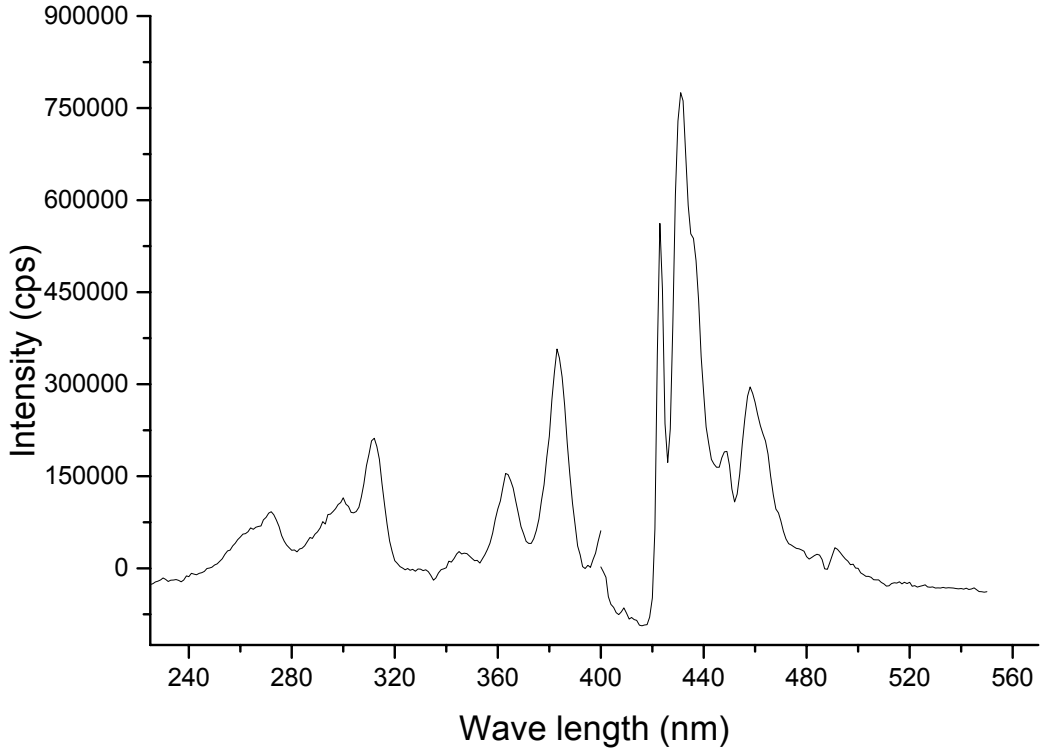

Figure 3.19 Excitation and fluorescence spectra of 20 ng/mL 3-OHb[a]p in 1-octanol at 77K

The 77K spectra were merely used as reference sources of excitation and emission wavelengths for 4.2K measurements. Liquid helium temperature measurements were performed with the cryogenic fiber optic probe and the multidimensional laser system. The slit width of the spectrograph was kept to a minimum (40μm) to reach the limiting resolution of the instrumental system, i.e. 0.32 – 0.40 nm. [74] Site-selective excitation was not attempted. Figures 3.20 to 3.23 compare the 4.2K fluorescence spectra of the four metabolites in their corresponding alcohols (A) to those in n-alkanes (B) of the same alkyl chain length. All spectra in alcohol solutions reveal characteristic vibrational structures similar to those usually observed from PAH/n-alkane systems. As shown in

Table 3.13, the improved spectral resolution increases the number of target wavelengths available for qualitative analysis of OH-PAH.

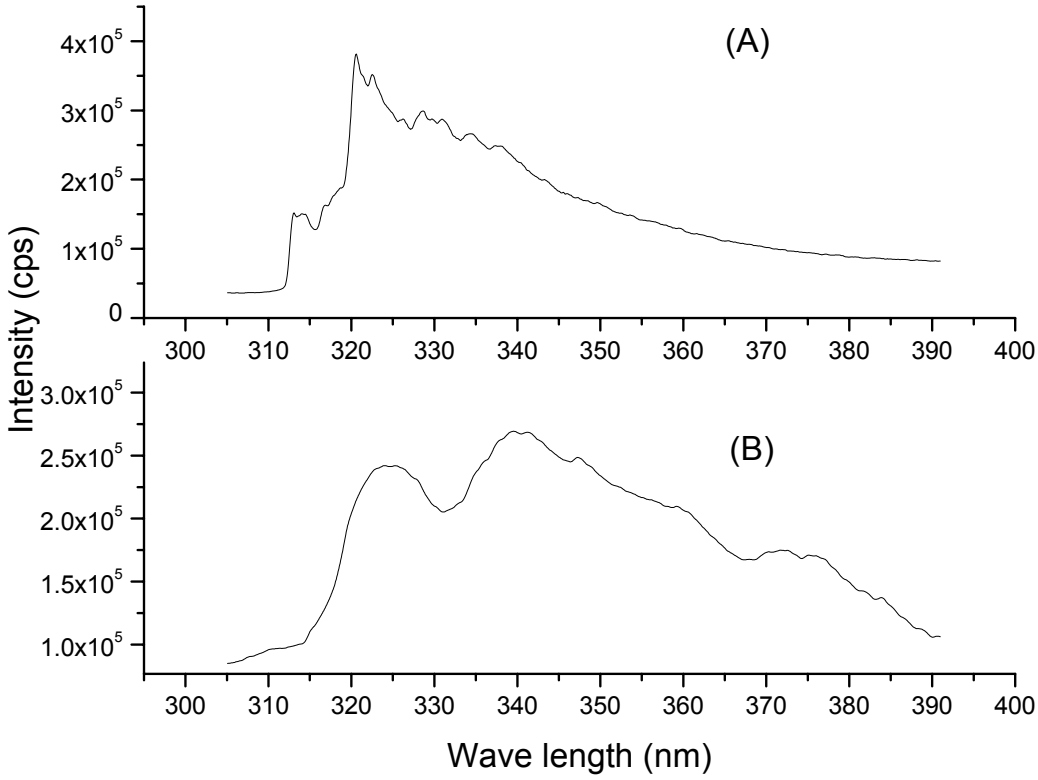

Figure 3.20. 4.2K fluorescence spectra of 2-OHflu in 1-heptanol (A) and n-heptane (B)

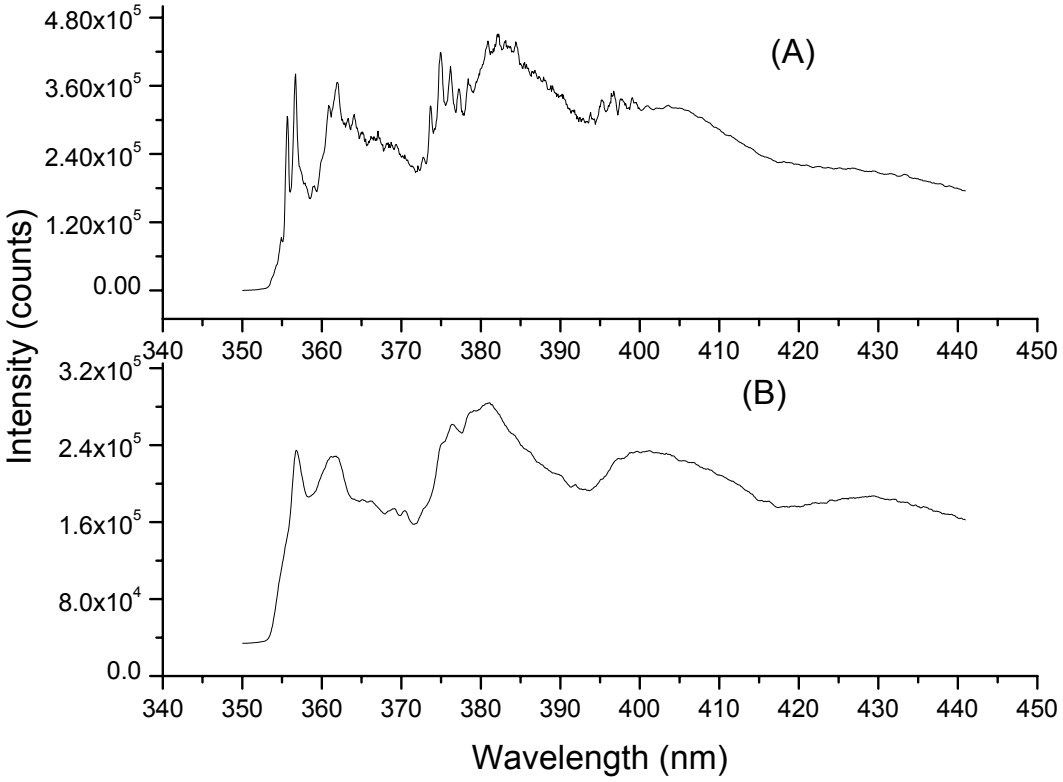

Figure 3.21. 4.2K fluorescence spectra of 9-OHphe in 1-hexanol (A) and n-hexane (B)

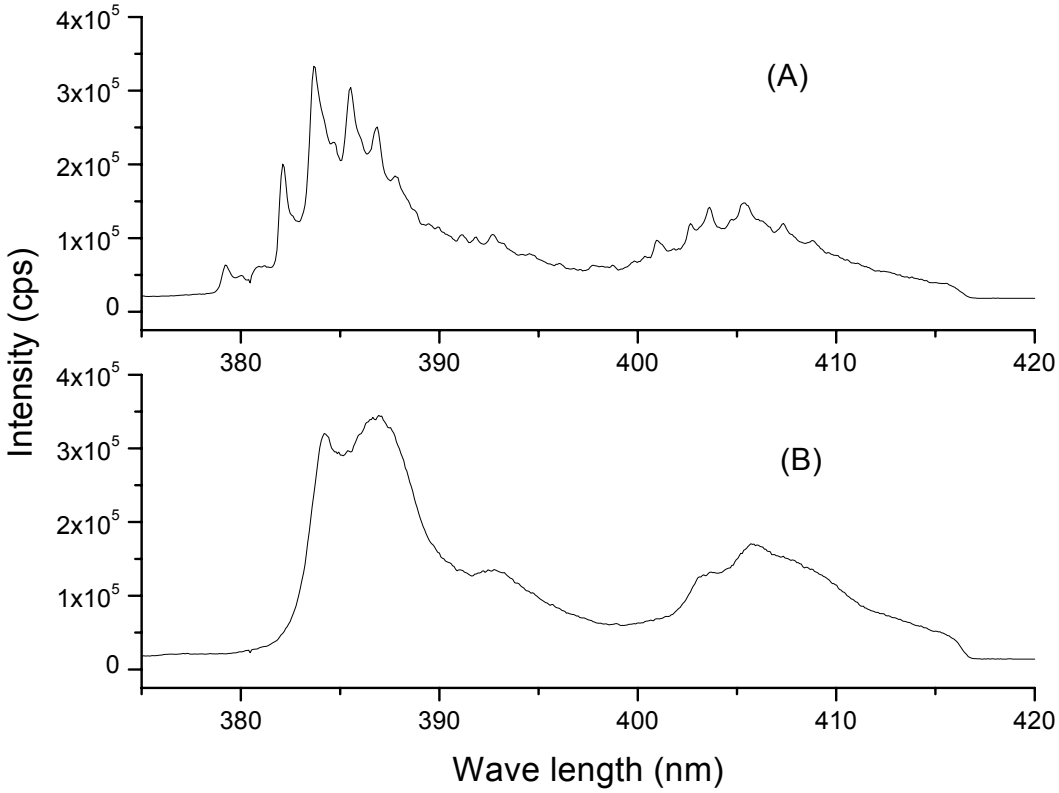

Figure 3.22. 4.2K fluorescence spectra of 1-OHpyr in 1-hexanol (A) and n-hexane (B)

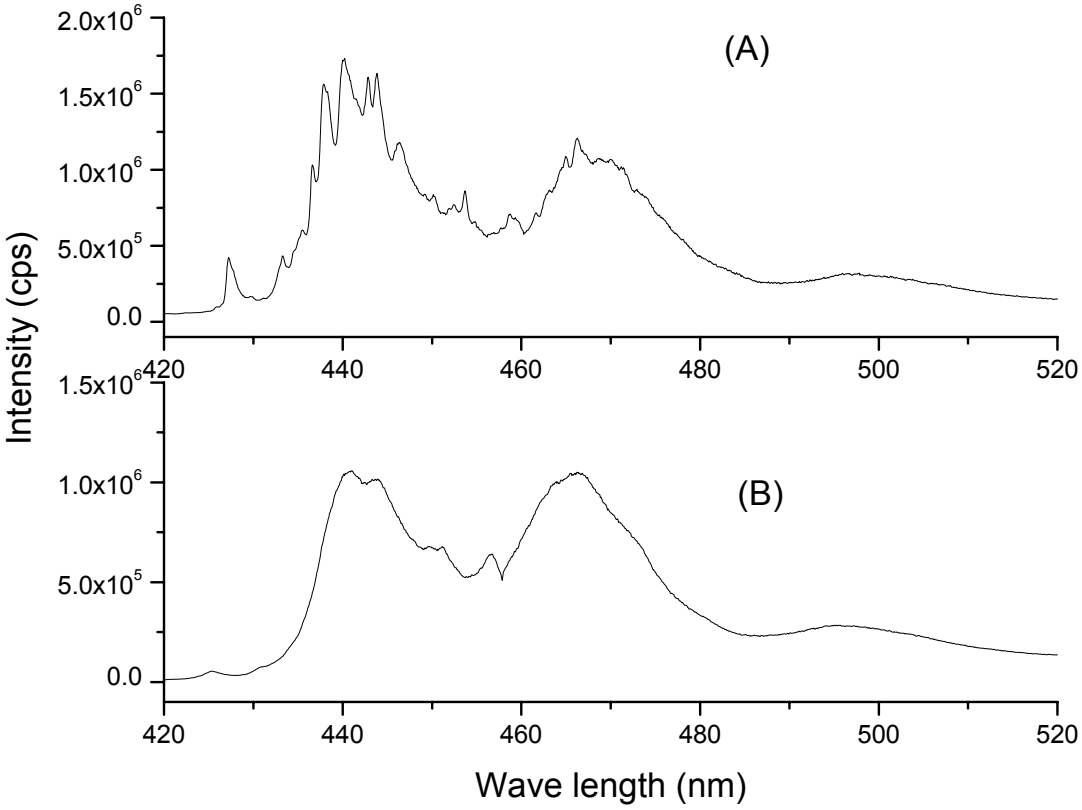

Figure 3.23. 4.2K fluorescence spectra of 3-OHb[a]p in 1-octanol (A) and n-octane (B)

Table 3.13. 4.2K Excitation and Emission Wavelengths of OH-PAH

PAHm	λ_{ex}[a] *(nm)*	*Alkane* λ_{em}[b] *(nm)*	*Alcohol* λ_{em} *(nm)*
1-OHpyr	347.9	384.2, <u>386.7</u>	380.2, <u>383.5</u>, 385.4, 386.9
2-OHflu	293.6	<u>324.1</u>, 340.2	313.6, <u>320.8</u>, 328.5
3-OHb[*a*]p	311.5	<u>443.1</u>, 458.9, 468.6	<u>430.2</u>, 437.6, 440.3, 442.7, 453.1
9-OHphe	307.1	356.4, 361.3, <u>380.7</u>	356.7, <u>361.9</u>, 374.8, 382.1, 396.8

[a] – Wavelength of excitation.
[b]- Wavelength of emission used for identification.
Underline indicates that it is the maximum emission wavelength.

3.5.2. 4.2K LETRSS Analytical Figures of Merit OH-PAH Metabolites in Alcohol Systems

Figures **3.24-3.27** show the fluorescence decays as a function of time "striped" from the 4.2K WTM of the four metabolites at their respective excitation and fluorescence maximum wavelengths. The four data sets fit well-behaved single exponential decays that provide distinct fluorescence lifetimes for the studied metabolites.

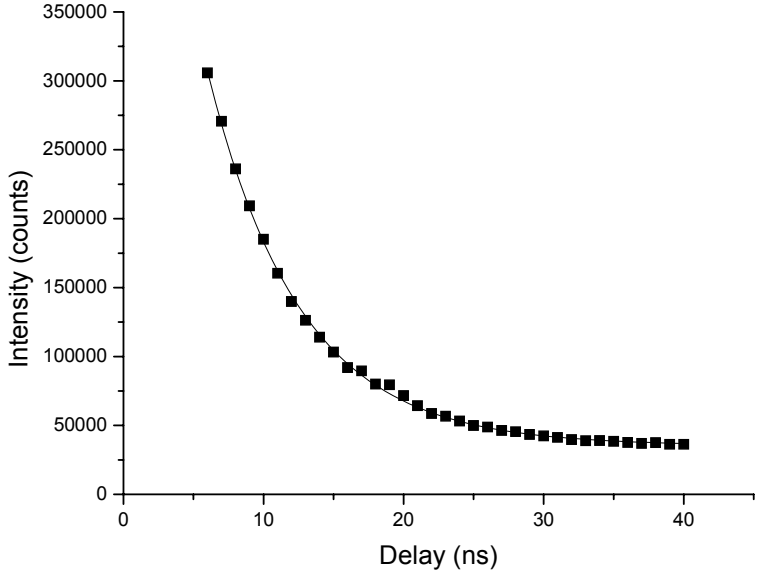

Figure 3.24. 4.2K fluorescence decay of 2-OHflu in 1-heptanol

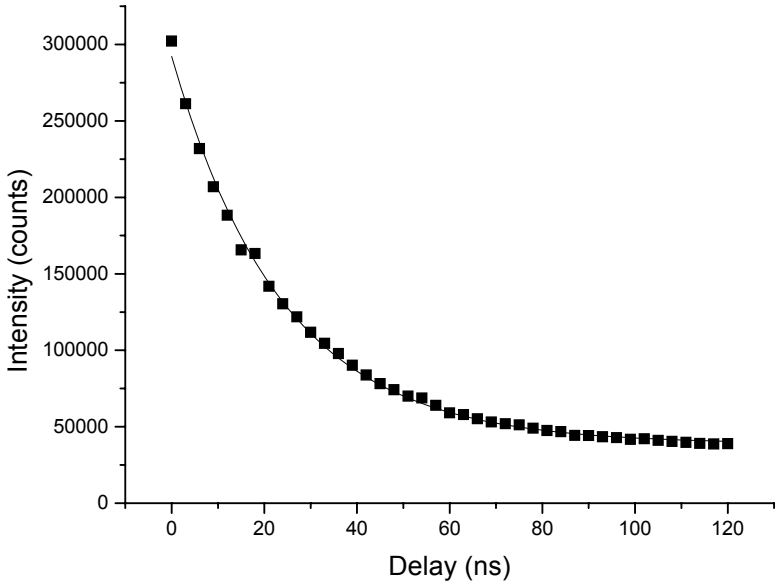

Figure 3.25. 4.2K fluorescence decay of 9-OHphe in 1-hexanol

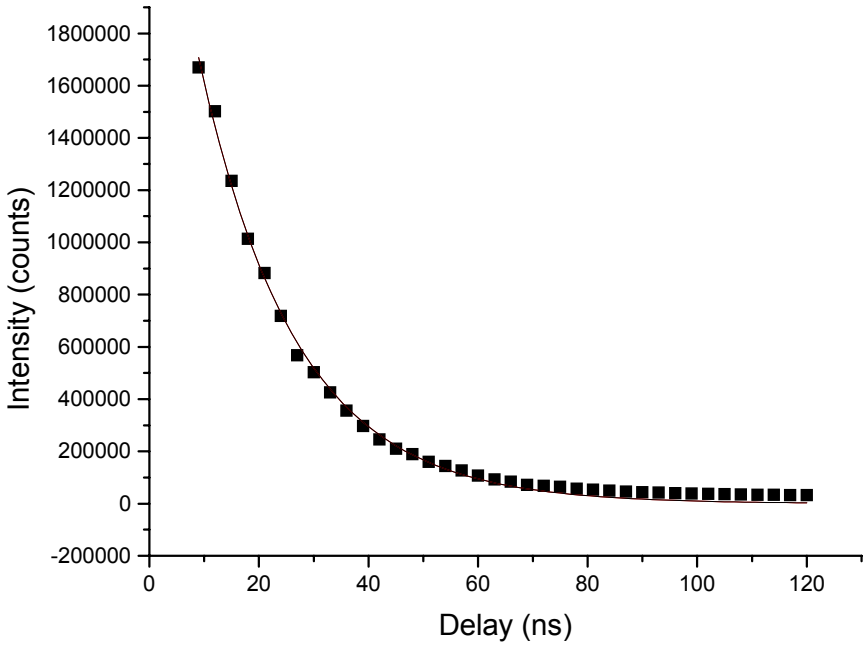

Figure 3.26. 4.2K fluorescence decay of 1-OHpyr in 1-hexanol

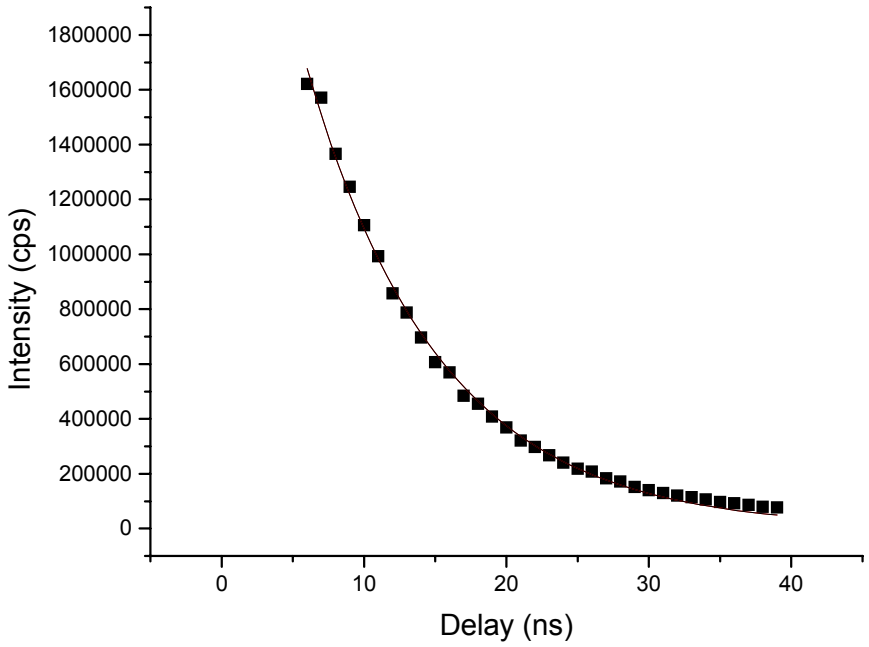

Figure 3.27. 4.2K fluorescence decay of 3-OHb[a]p in 1-octanol

The 4.2K fluorescence lifetimes are listed in Table 3.14 with the remaining 4.2K LETRSS-AFOM. The significant differences in the lifetime values enhance the selective potential of the technique for the qualitative analysis of the studied metabolites. The comparison of the LOQ to those reported in **Table 3.4** show an improvement of approximately one order of magnitude. When making this comparison, one should take into consideration the fact that different instrumental set ups were used for RT and 4.2K measurements. A straightforward comparison to elucidate the effects of solvent and temperature in the AFOM of the studied metabolites should only be possible with measurements carried out with the same instrumental set up. Keeping in mind the pre-concentration factor of SPE (~ 3x), the combination of SPE to 4.2K LETRSS should make feasible the determination of OH-PAH at the $pg.mL^{-1}$ concentration level.

Table 3.14. 4.2K Analytical Figures of Merit[e] of PAH metabolites in respective shpol'skii alcohols.

PAHm	$\lambda_{ex/em}$[a]	*Life time (ns)*	LDR[b]	R^{2}[c]	LOD[d]	LOQ[e]
2-OHflu	293.6/320.8	4.33 ± 0.11	0.136-15	0.9946	0.041	0.136
9-OHphe	307.1/361.8	10.22 ± 0.19	0.184-20	0.9930	0.056	0.184
1-OHpyr	347.9/380.2	10.77 ± 0.29	0.04-10	0.9978	0.012	0.040
3-OHb(a)p	311.5/430.2	13.30 ± 0.49	0.056-10	0.9961	0.017	0.056

[a] Maximum excitation and emission wavelength in nm.

[b] Linear dynamic range in ng/mL

[c] Limit of detection (ng/mL) is calculated from 3 × standard deviation(s_b) of sixteen blank measurements divided by slope(m) of the calibration curve.

[d] Limit of Quantification (ng/mL) is calculated from $10s_b/m$

[e] Estimated using emission slits of 500 nm, and optimum delay (10 ns) and gate time (1000 ns)

CONCLUSION

A few attempts have been published in the literature towards the screening of PAH metabolites. Due to the strong luminescence resulting from the rigid and delocalized π-electron system of OH-PAH, screening methods have centered on either RTF spectroscopy or Solid-Surface Room-Temperature Phosphorescence (SS-RTP) spectroscopy. While RTF spectroscopy was applied to the analysis of 1-hydroxypyrene glucuronide, a conjugate of 1-hydroxypyrene and index biomarker for mixed PAH exposure, [75] the SS-RTP method was developed to determine benzo[*a*]pyrene-r-7,t-8,9,10-tetrahydro-tetrol, a metabolite of benzo[*a*]pyrene, which is the most carcinogenic PAH in the EPA list. [76] RTP was enhanced with thallium acetate, an external heavy-atom source known to promote intersystem crossing from the first singlet excited state to the triplet state manifold. Both methods minimize spectral interference via synchronous excitation, which consists of varying simultaneously both the excitation (λ_{exc}) and emission (λ_{em}) wavelengths while keeping a constant wavelength interval ($\delta\lambda = \lambda_{em} - \lambda_{exc}$) between them. Urine clean-up and metabolite pre-concentration were carried out via immunoaffinity [75] or metabolite adsorption on C-18 bonded silica particles imbedded in Whatman 42 filter paper disks. [76]

Our approach - SPE-RTF EEM spectroscopy – takes a step forward into screening methodology making possible the direct determination of six OH-PAH in urine samples. Keeping in mind that spectral overlapping is resolved via U-PLS/RBL, i.e. a robust chemometric algorithm capable to handle more than six metabolites, it is possible to envision the application of SPE-RTF EEM spectroscopy to a much larger number of OH-PAH. Its straightforward experimental procedure is well-suited for routine analysis of

numerous samples. SPE is carried out on commercially available C18 cartridges via an optimized extraction procedure that minimizes metabolite loss. PAH metabolites are directly determined in the eluting solvent (3mL of methanol) without the need of previous solvent evaporation. Excellent recoveries were obtained for all studied biomarkers, which varied from 88.5 ±1.31 % (9-OHphe) to 99.8 ± 1.04 (3-OHb[a]p). For 10mL of urine samples, LOD varied between 0.01ng.mL^{-1} (3-OHb[a]p) and 0.6ng.mL^{-1} (2-OHnap). These LOD are of the same order of magnitude as those reported via HPLC (see Table 1.2). Future attempts to improve LOD should consider the main source of fluorescence background, which consist on the fluorescence impurities of SPE cartridges that co-elute with OH-PAH in the eluting solvent. Background reduction might be achieved by flushing the SPE cartridge with methanol prior to sample loading.

1-OHpyr, 9-OHphe, 2-OHflu and 3-OHb[a]p showed clear resolution improvements in their 4.2K fluorescence spectra when dissolved in an alcohol of appropriate molecular length. Lifetime analysis provided well-behaved single exponential decays with distinct fluorescence lifetimes for peak identification and peak purity check in Shpol'skii spectra of complex samples. The improved spectral resolution and well-behaved single exponential decays reduce the number of potential interference and simplifies the application of PARAFAC, an algorithm with the 2nd order advantage. In comparison to RTF, 4.2K LETRSS showed LOQ improvements of approximately one order of magnitude. Keeping in mind the pre-concentration factor of SPE (~ 3x), the combination of SPE to 4.2K LETRSS should make feasible the determination of OH-PAH at the pg.mL^{-1} concentration level.

The fact that both approaches are not destructive makes them well-suited tools for screening OH-PAH metabolites in urine samples. The information obtained via SPE-RTF EEM spectroscopy and/or 4.2K LETRSS spectroscopy can be very useful in setting priorities for more detailed and costly studies via intricate analytical protocols and sophisticated techniques.

APPENDIX A: EEM OF OH-PAH METABOLITES

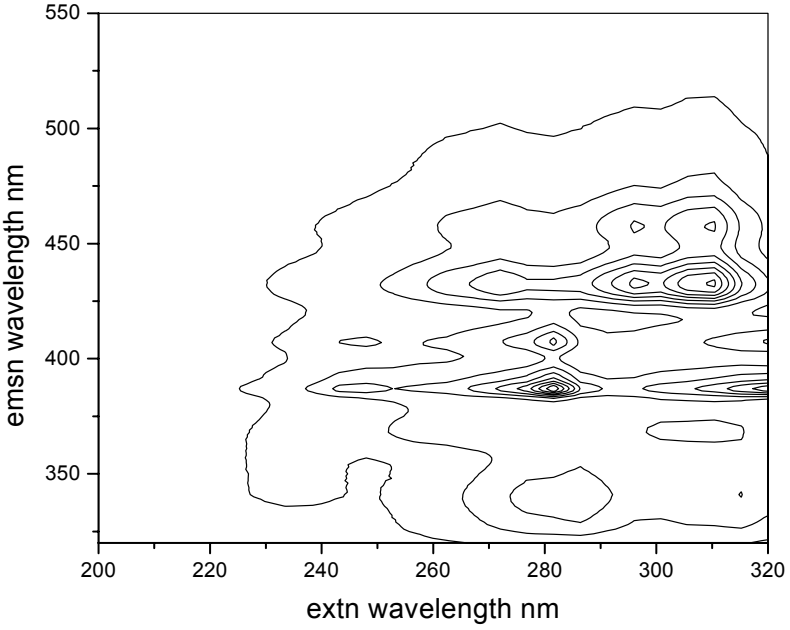

Figure A.1 EEM spectra of standard sample 1

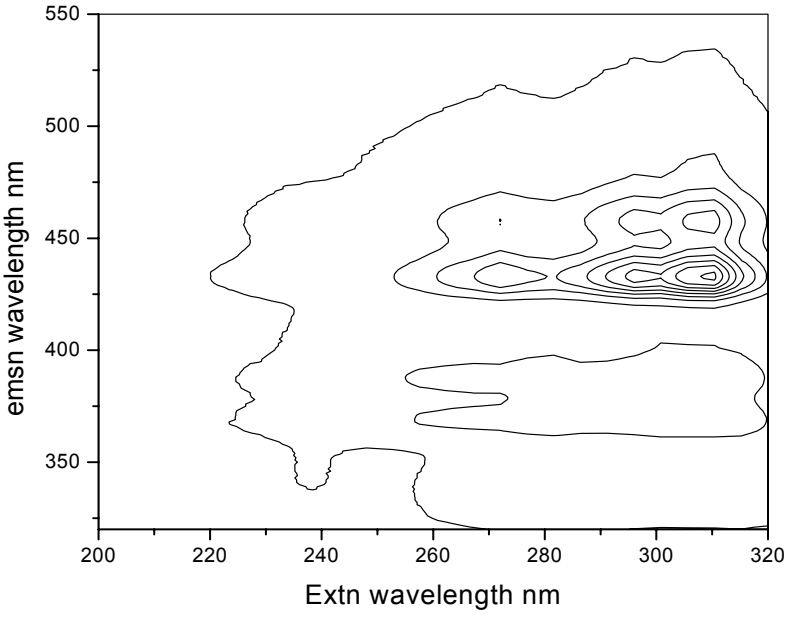

Figure A.2 EEM spectra of standard sample 2

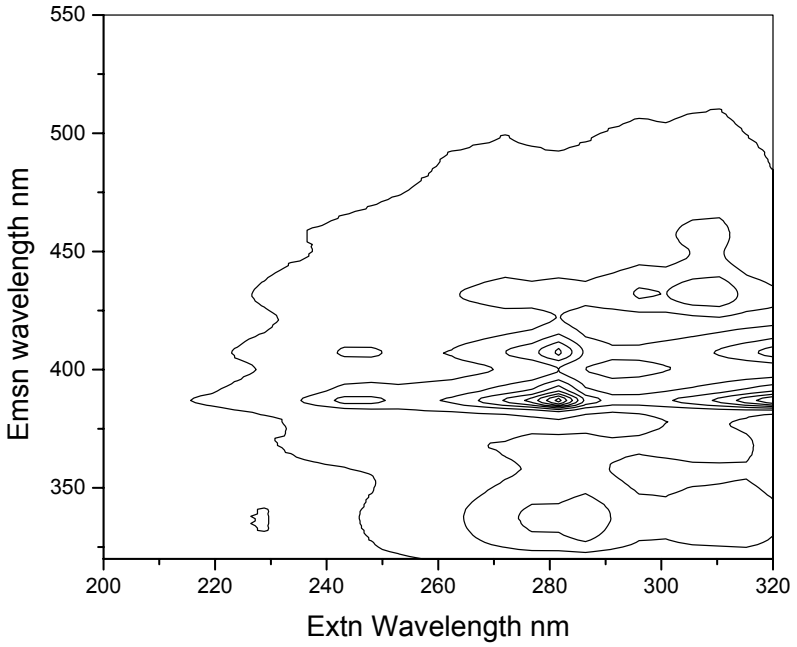

Figure A.3 EEM spectra of standard sample 3

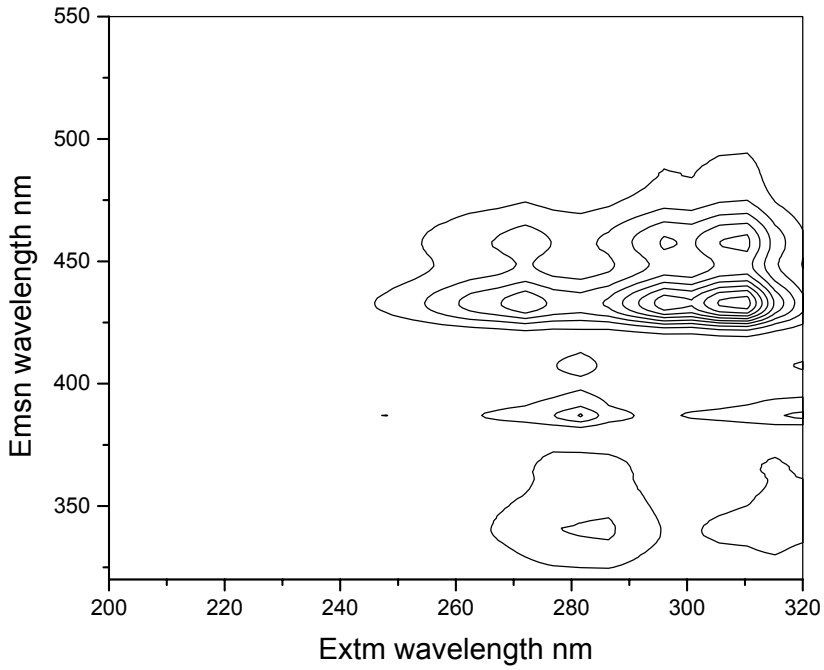

Figure A.4 EEM spectra of standard sample 4

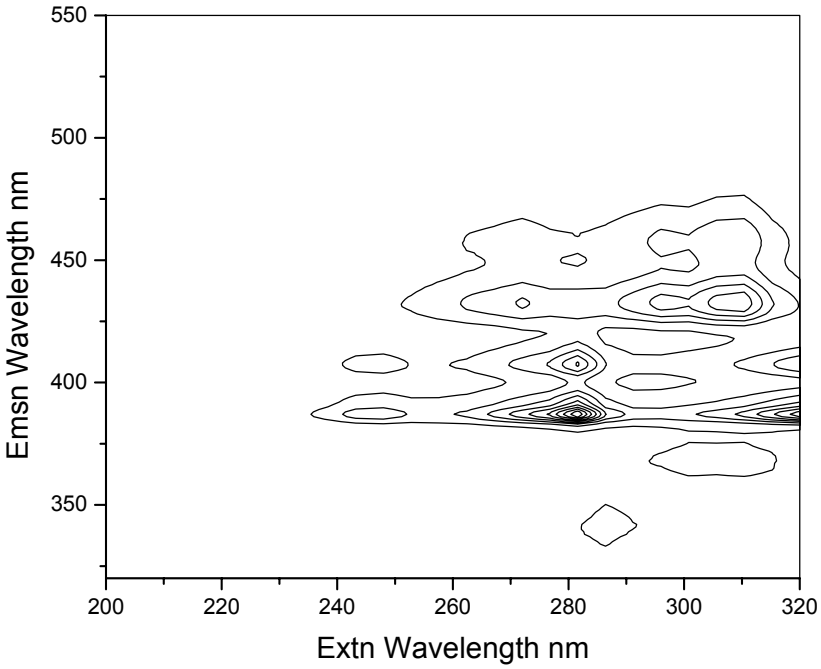

Figure A.5 EEM spectra of standard sample 5

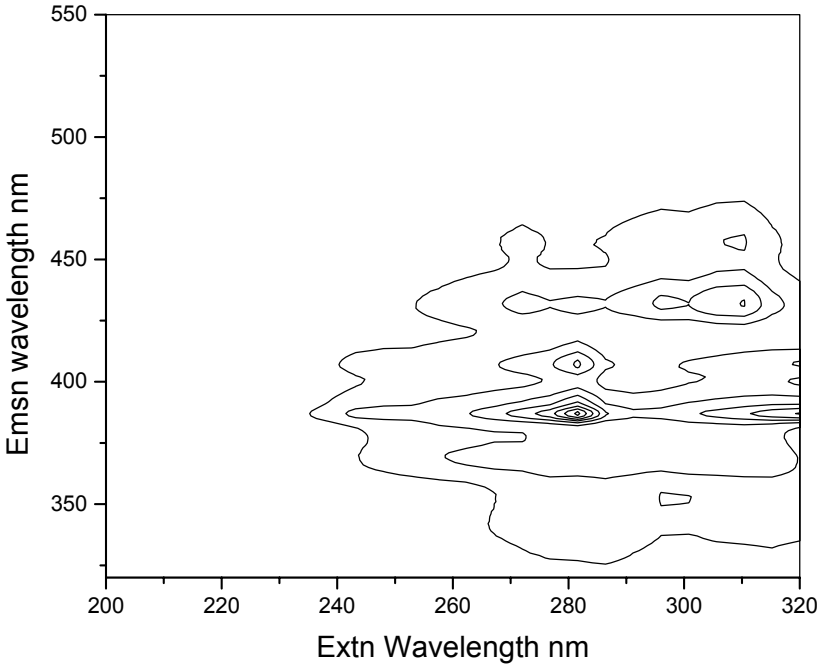

Figure A.6 EEM spectra of standard sample 6

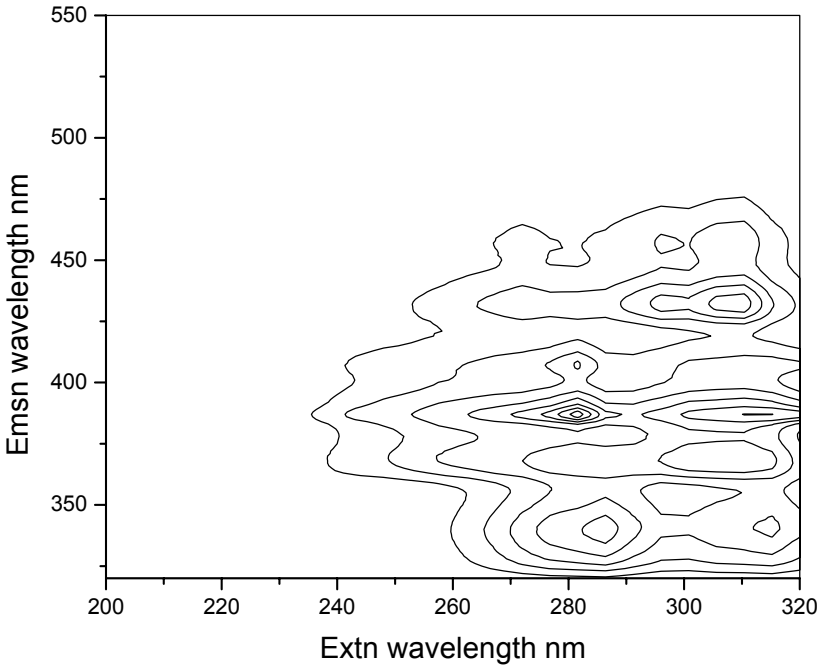

Figure A.7 EEM spectra of standard sample 7

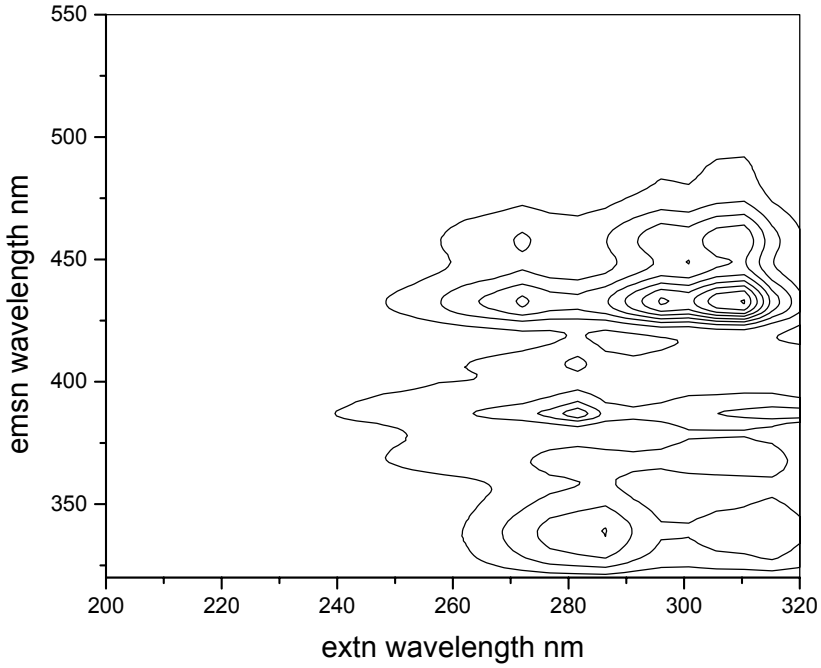

Figure A.8 EEM spectra of standard sample 8

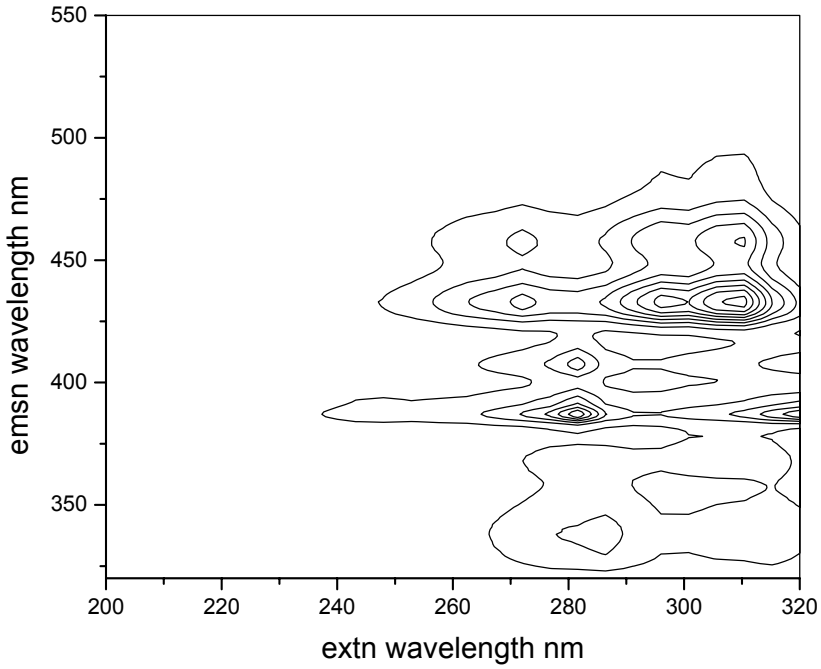

Figure A.9 EEM spectra of standard sample 9

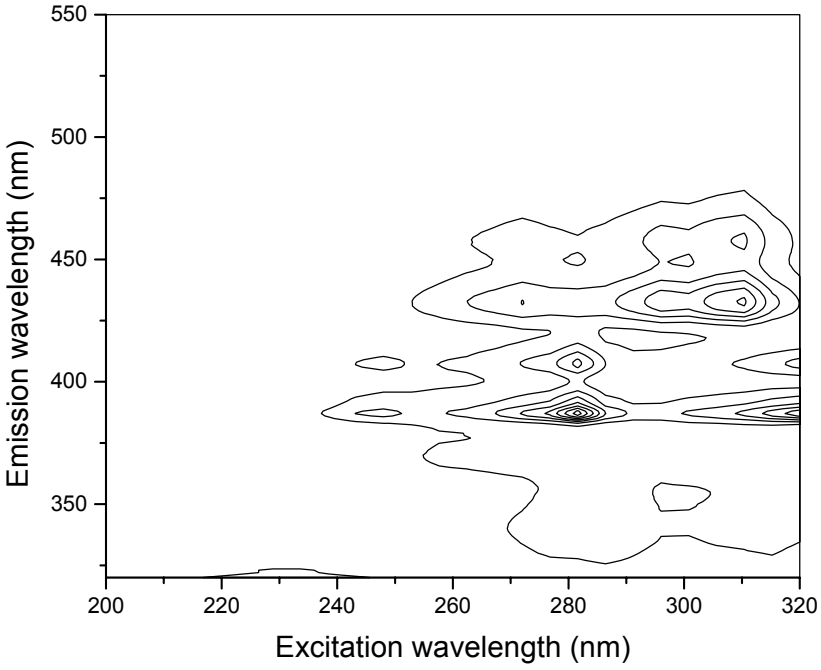

Figure A.10 EEM spectra of validation 1

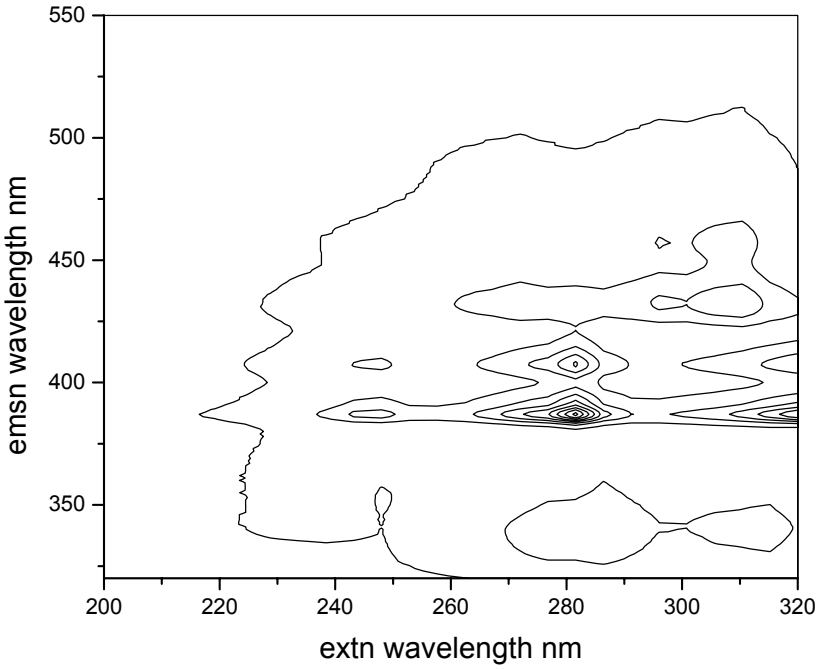

Figure A.11 EEM spectra of validation 2

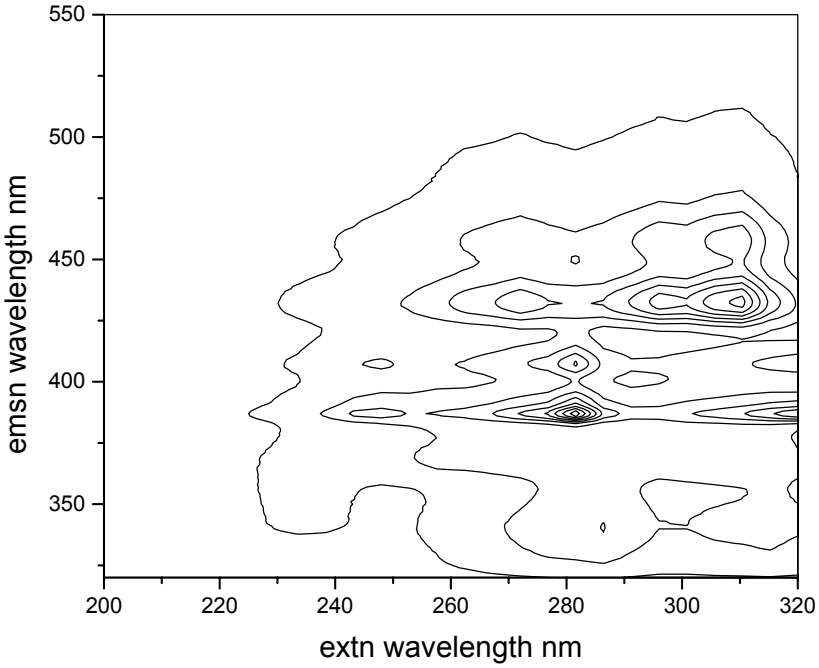

Figure A.12 EEM spectra of validation 3

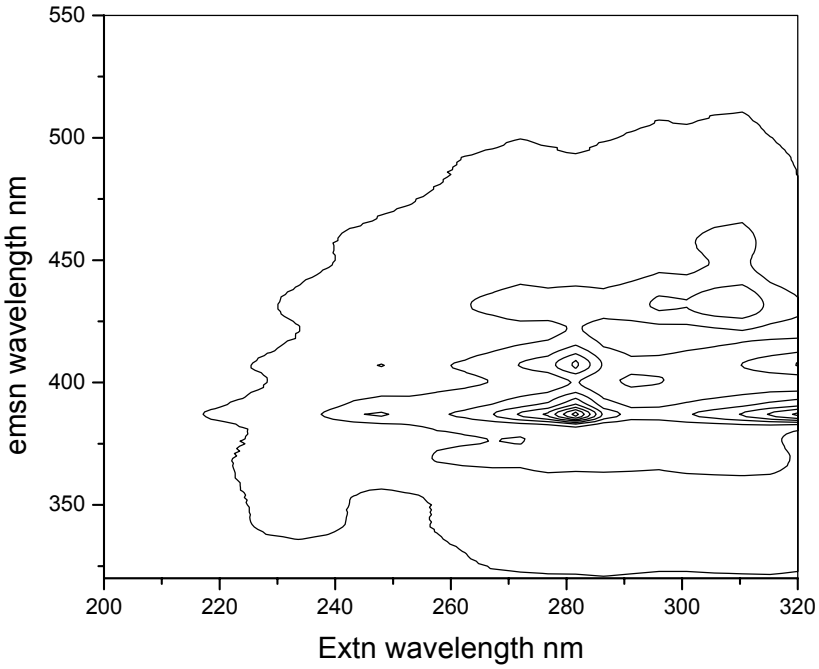

Figure A.13 EEM spectra of validation 4

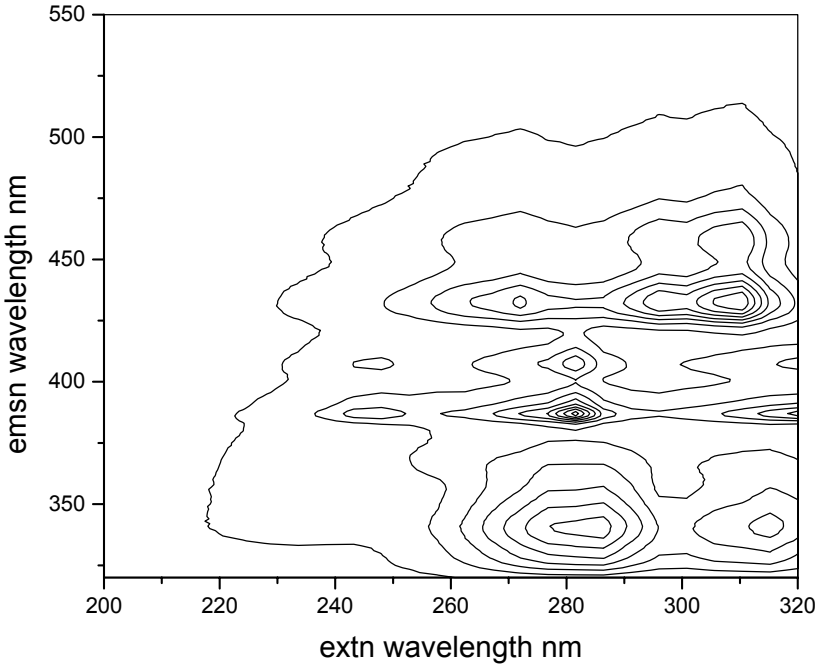

Figure A.14 EEM spectra of validation 5

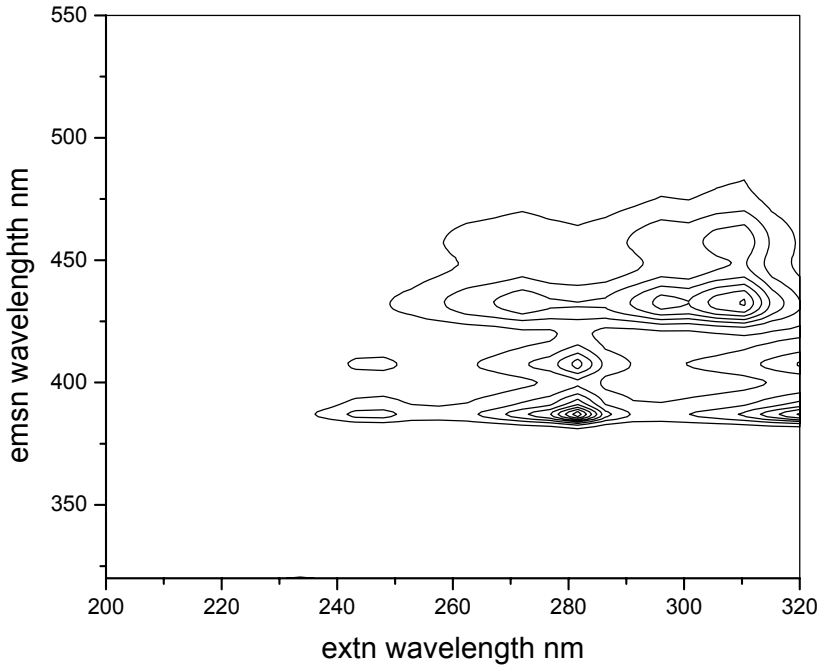

Figure A.15 EEM spectra of validation 6

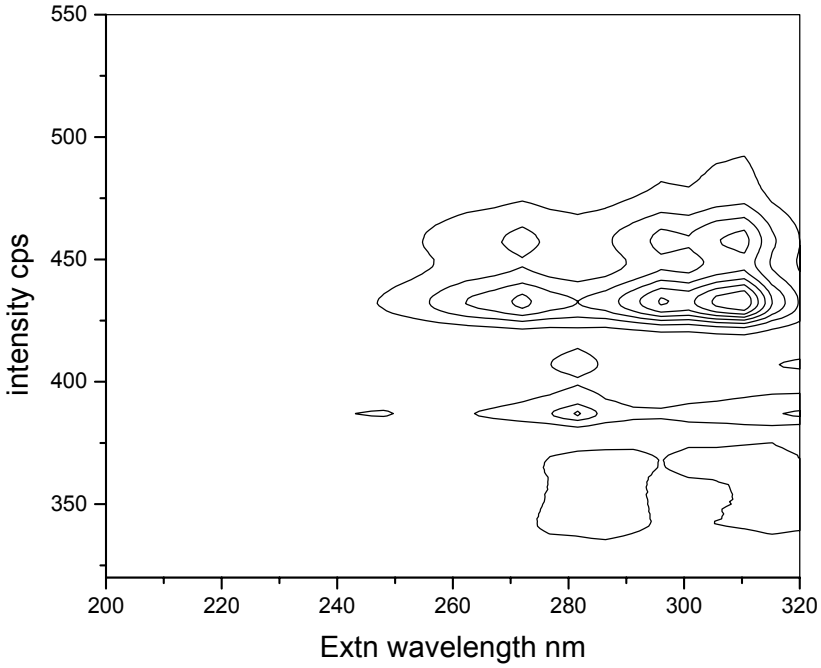

Figure A.16 EEM spectra of validation 7

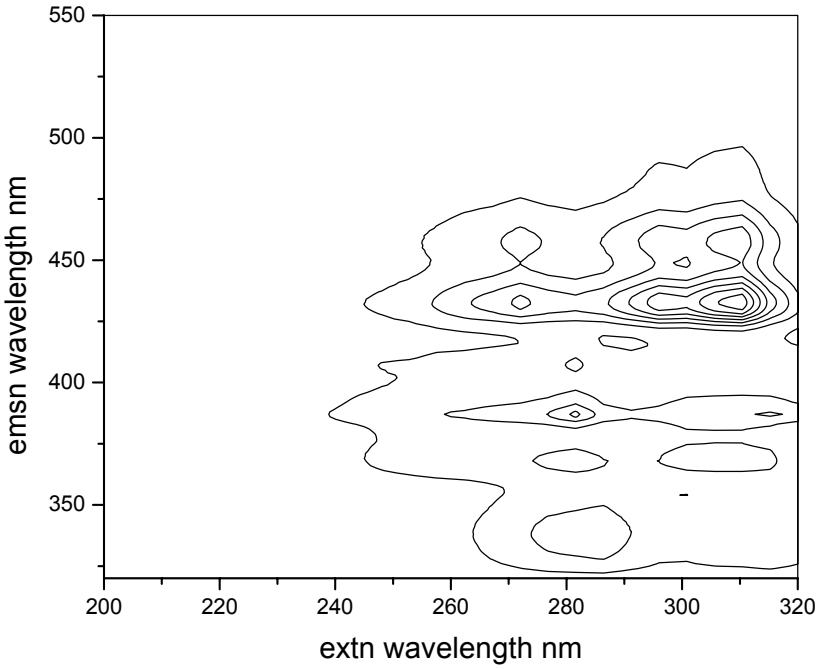

Figure A.17 EEM spectra of validation 8

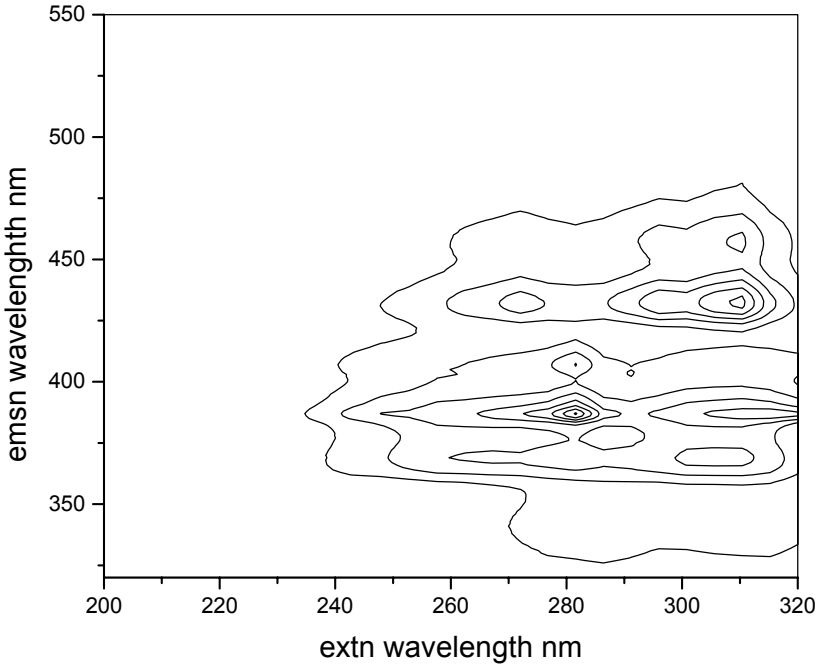

Figure A.18 EEM spectra of validation 9

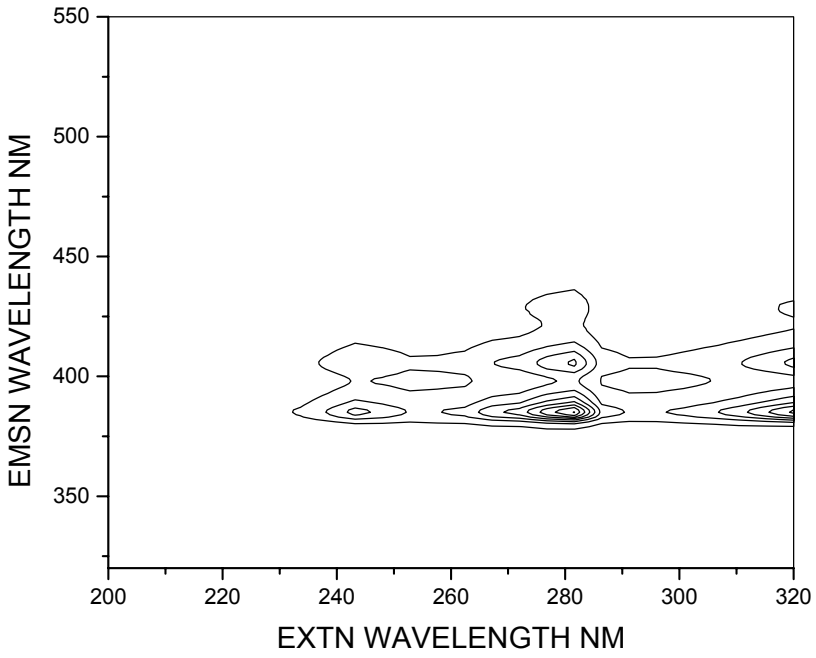

Figure A.19 EEM spectra of Sample Mixture 1.

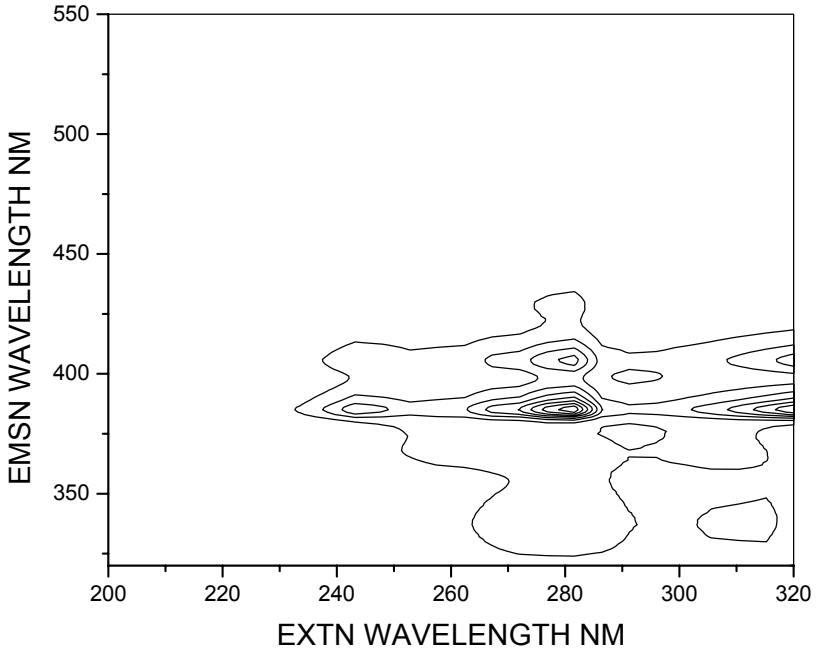

Figure A.20 EEM spectra of Sample Mixture 2.

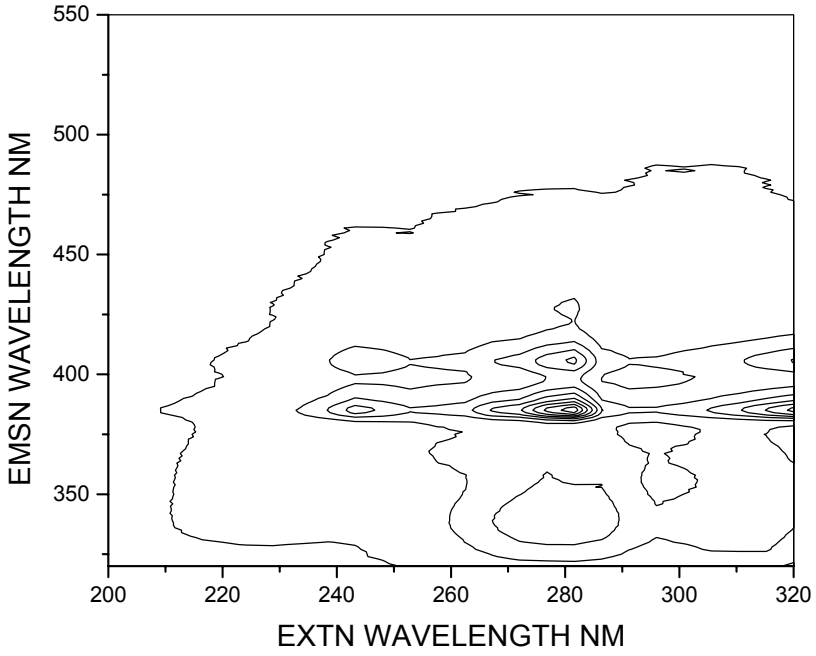

Figure A.21 EEM spectra of Sample Mixture 3.

LIST OF REFERENCES

1. Polycyclic Aromatic Hydrocarbons, U.S. Department of Health and Human services, *Ninth report on carcinogen*s, **2001**

2. T. Vo-Dinh, A.D.Campiglia, **1998**, *Talanta*, *47*, 943-969.

3. Yu Wang, Wenbing Zhang, *Anal . Bioanal. Chem,* **2005,** *383*, 804-809

4. Ching-Tang Kuo, *Journal of Chromatography B*, 805, **2004**, 187-193.

5. Leea Kuusimaki, *Int Arch Occup Environ Health*, **2004**, 77, 23-30

6. Lovisa C. Romanoff, *Journal of Chromatography B*, 835, **2006**, 47-54.

7. Christopher J.Smith, *Journal of Chromatography B*, 778, **2002**, 157- 164.

8. B. Serdar, *Environ. Health Perspect.* **111** (**2003**), pp. 1760–1764.

9. Frans J. Jongeneelen*, Environment & Health*, **1986**, 12, 137-143.

10. Frans J. Jongeneelen, *International Archives of Occupational & Environmental Health*, **1985**, 57, 47-55.

11. Grimmer G, *Archives of Toxicology*, **1988**, 62(6), 401-405.

12. Yinghe Li, *Rapid Commun. Mass Spectrom*. **2005**, 19, 3331-3338.

13. Gmeiner, G.; *Journal of Chromatography B*, 705 (1), **1998**, 132-138(7).

14. Thurman, E.M,. Mills, M.S., *Solid Phase Extraction: Principles and Practice*, John Wiley & Sons, New York, **1988**.

15. Dorsey, J.G., Cooper, W.T., *Anal.Chem*., 66, 1994, 857

16. Larrive, M.L., Poole, C.F. *Anal. Chem*., 66, **1994**,139

17. Mayer, M.L., Poole, C.F., *Anal Chim. Acta.,* 294, **1994**, 113.

18.Winefordner, J.D., Schulman, S.G., O'Haver, T.C. *Luminescence Spectroscopy in Analytical Chemistry*, Wiley-Interscience, New York, **1972**.

19. Schulman, S.G., *Molecular Luminescence Spectroscopy and Applications: part1&2,* Wiley-Interscience, New York, **1985**.

20. Hurtubise, R.J., *Molecular Phosphorimetry: Theory, Instrumentation and Applications*, VCH Publishers, New York, **1990**.

21. Vo Dinh, T., *Room Temperature Phosphorimetry for Chemical Analysis*, Wiley-Interscience, New York, **1984**.

22. Melhuish, V.H., Zander, M., *Pure & Appl. Chem*., 53, **1981**, 1953.

23. Schulman, E.M., *J. Chem. Educ*., 53, **1976**, 522.

24. Knorr, F.J., Harris, J.M. *Anal. Chem*. **1981**, 53,272-276.

25. McGown, L.B. *Anal. Chem*. **1989**, 61, 839A – 847A.

26. Smalley, M.B., Shaver, J.M., *Anal. Chem*. **1993**, 65, 3466-3472.

27. Ho, C.N., Warner, I.M. *Anal. Chem*. **1982**, 54, 2486-2491.

28. Warner, I.M., Patonay, G., *Anal. Chem*. **1985**, 57, 463A – 483A.

29. T. Vo-Dinh, *New Directions in Molecular Luminescence,* ASTM, Philadelphia, PA, **1983**, p.5.

30. T. Vo-Dinh, P.R. Martinez, *Anal. Chim. Acta* 125,**1981**,13.

31. T. Vo-Dinh, R.B. Gammage, *Anal. Chem*. 53, **1981**, 253.

32. P. Garrigues and M. Ewald, *Intl. J. Environ. Anal. Chem*. 21, 185-197, **1985.**

33. W. Karcher, J. Devillers, *Spectral Atlas of Polycyclic Aromatic Compounds*, Vol. 3. The Netherlands, **1991**, 1092.

34. F. Ariese, S.J. Kok, *Anal. Chem*., 65, 1100-1106, **1993**.

35. Cees Gooijer, *Chemical Analysis*, Vol. 156, Wiley-Interscience, New York, **2000**.

36. J. W, Hofstraat, *J. Phys. Chem*. 93, 184-190, **1989**.

37. S.J. Weeks, *Anal. Chem*. 62,1472-1477,**1990**.

38. S.J. Weeks, *Appl. Spectr*. 45,1093-1100,**1991**.

39. E. D. Hagestuen and A. D. Campiglia, **1999**, *Talanta,* 49, 5476-560.

40. A. F. Arruda and A. D. Campiglia, **2000**, *Environmental Science and Technology*, 34, 4982-4988.

41. J. L. Whitcomb and A. D. Campiglia, **2001**. *Talanta,* 55, 509-518.

42. J. L. Whitcomb, A. J. Bystol, A. D. Campiglia, **2002**, *Anal. Chimica Acta* 464, 261-272.

43. Brochure or manual of SPE cartridge. Information provided to you by commercial source.

44. *Statistics for Analytical Chemistry*, J. C. Miller, Chichester: Ellis Horwood, **1993**.

45. J. L. Long and J. D. Winefordner, *Anal. Chem*. 55, 713A, **1983**.

46 Yu Wang, Wenbing Zhang, *Anal. Bioanal Chem,* **2005,** *383*, 804-809

47. *A Series of Monographs on Analytical Chemistry and its Applications*, J. D. Winefordner, Series Editor. pp 37-138.

48. D. Patra and A. Mishra, *Talanta*, 55, 143-153, **2001**.

49. M. L. Nahorniak and K. S. Booksh, *Analyst*, 131, 1308-1315, **2006**.

50. R. Bro, *Chemom. Intell. Lab. Syst*., 38, 149-171, **1997**.

51. A. K. Smilde, *Chemom. Intell. Lab. Syst*., 15, 143 – 157, **1992**.

52. Wold S, Geladi P, Esbensen K, Øhman J., *J. Chemometrics* **1987**, *1*, 41–56.

53. Öhman, J., Geladi, P, Wold, S. *J. Chemometrics*, **1990**, *4*, 79–90

54. Olivieri, A.C. *J. Chemometris*, **2005**, *19*, 253–265.

55. Gil DB, Arancibia JA, *Anal. Chem* 78 (23): 8051-8058, **2006**

56.Culzoni, M.J.; Goicoechea, H.C.; Bearzoti, M.; Cabezón, M.; Olivieri, A.C., *Analyst* **2006**, *131*, 718–723.

57. Olivieri, A.C.; Goicoechea, H.C.; Iñón, F.A., *Chemom. Intell. Lab. Syst.* **2004**, *73*, 189–197.

58. Wold S, Geladi P, Esbensen K, Øhman J., *J. Chemometrics* **1987**, *1*, 41–5.

59. Haaland, D.M.; Thomas, E.V., *Anal. Chem*. **1988**, *60*, 1193–1202.

60. A. R. Muroski, K. S. Booksh and M. L. Myrick, *Anal. Chem*. 68, 3534 – 3538, 1996.

61. A. R. Muroski, K. S. Booksh and M. L. Myrick, *Anal. Chem*. 68, 3539 – 3544, 1996.

62. A. D. Campiglia, A. J. Bystol, S. Yu, **2006**, *Analytical Chemistry* 78(2), 484-492.

63. A. D. Campiglia, S. Yu., A. J. Bystol, H. Wang, **2007,** *Analytical Chemistry*, 79(4), 1682-1689.

64. Bystol A. J., Campiglia A. D., Gillispie G. D., *Applied Spectroscopy* **2000**, 54, 910.

65. Bystol A. J., Whitcomb J. L., Campiglia A. D., *Environmental Science & Technology* **2001**, 35, 2566 - 2571.

66. Martin T. L., Campiglia A. D., *Applied Spectroscopy* **2001**, 55, 1266 - 1272.

67. Bystol A. J., Campiglia A. D., Gillispie G. D., *Analytical Chemistry* **2001**, 73, 5762 - 5770.

68. Bystol A. J., Thorstenson T., Campiglia A. D., *Environmental Science & Technology* **2002**, 36, 4424 - 4429.

69. Martin T. L., Arruda A. F., Campiglia A. D., *Applied Spectroscopy* **2002**, 56, 1354-1360.

70. Arruda A. F., Yu S., Campiglia A. D., *Talanta* **2003**, 59, 1199 - 1211.

71. Bystol A. J., Yu S., Campiglia A. D., *Talanta* **2003**, 60, 449 - 458.

72. Bystol A. J., Campiglia A. D., *Applied Spectroscopy* **2003**, 57, 697 - 702.

73. Campiglia A. D., Bystol A. J., Yu S., *Analytical Chemistry* **2006**, 78, 484 - 492.

74. Campiglia A. D., Yu S., Bystol A. J., Wang H., *Analytical Chemistry* **2007**, 79, 1682 - 1689.

75. Watson G.M., *Aquatic toxicology*, 67 (2): 127-142, **2004**

76. M. Uziel, G. H. Miller, R. Ward, W. Watts and T. Vo-Dinh, Polycyclic Aromatic Compounds, 3, 12-27, **1992**.